IEEE Access
Multidisciplinary ⋮ Rapid Review ⋮ Open Access Journal

Received 19 January 2023, accepted 23 February 2023, date of publication 6 March 2023, date of current version 22 March 2023.

Digital Object Identifier 10.1109/ACCESS.2023.3253380

RESEARCH ARTICLE

Efficient Numerical Solution of Coupled Axisymmetric Plasma Equilibrium and Eddy Current Problems

MATTEO BONOTTO[1,2], DOMENICO ABATE[1], PAOLO BETTINI[1,3], (Senior Member, IEEE), ANTONIO IAIUNESE[4], NICOLA ISERNIA[5], AND FABIO VILLONE[5]

[1]Consorzio RFX (CNR, ENEA, INFN, University of Padua, Acciaierie Venete SpA), 35127 Padua, Italy
[2]INFN-LNL, 35020 Legnaro, Italy
[3]Dipartimento di Ingegneria Industriale (DII), University of Padua, 35131 Padua, Italy
[4]Centro Ricerche Fusione, University of Padua, 35127 Padua, Italy
[5]Consorzio CREATE, DIETI, University of Naples Federico II, 80138 Naples, Italy

Corresponding author: Matteo Bonotto (matteo.bonotto@igi.cnr.it)

ABSTRACT This paper presents an efficient numerical tool for solving the problem of transient nonlinear evolution of plasma equilibrium in presence of eddy currents. The code, named FRIDA-TD (FRIDA-*Time Domain*), and based on the existing FRIDA (FRee-boundary Integro-Differential Axisymmetric) code, exploits two different approaches for solving the elated nonlinear system of Partial Differential Equations (PDE): (i) Finite Element Method - Boundary Element Method (FEM-BEM) for plasma equilibrium, and (ii) Axisymmetric Volume Integral (AVI) formulation for eddy currents. The resulting FRIDA-TD is a fast and flexible tool suitable for engineering-oriented purposes, such as the design of Tokamak devices, set up of plasma operations, prediction of performance scenarios, and design of feedback control systems. FRIDA-TD is successfully validated at first with the well-established CarMa0NL code, and then against experimental data of the RFX-mod device.

INDEX TERMS Eddy currents, free-boundary equilibrium, Grad-Shafranov equation, magnetic confinement fusion, magnetohydrodynamics.

I. INTRODUCTION

The problem of transient nonlinear evolution of plasma equilibrium in presence of eddy currents is a key task in Magnetic Confinement Fusion (MCF), specifically concerning tokamak devices. Computer codes that address this task are of paramount importance, as they are used to set up discharge scenarios, study breakdowns, disruptions, and design both the layout of new machines and the feedback control systems.

During the last decades, many codes have been developed to solve the problem of transient nonlinear evolution of plasma equilibrium in presence of eddy currents. Among others, we mention PROTEUS [1], DINA [2], TSC [3], MAXFEA [4], CEDRES++ [5], and CREATE-NL+ [6], all assuming both the plasma and the external conductors to be axisymmetric. On the other hand, it is worth mentioning another code that differs from the previous ones, because it is based on an arbitrary three-dimensional description of the external conductors, the CarMa0NL [7] code.

This paper aims to present an extension of the existing FRIDA (FRee-boundary Integro-Differential Axisymmetric) code [8], which solves the static free-boundary plasma equilibrium problem. This novel tool, named FRIDA-TD, which stands for FRIDA-*Time Domain*, exploits the same strengths of the FRIDA code: (i) two different approaches for solving the elated nonlinear system of Partial Differential Equations (PDE), that are Finite Element Method - Boundary Element Method (FEM-BEM) for plasma equilibrium, and Axisymmetric Volume Integral (AVI) formulation for eddy currents, requiring to mesh only the conductors and the vacuum chamber; (ii) it is based on a novel FEM-BEM coupling scheme which has been proven to have optimal convergence rate and

The associate editor coordinating the review of this manuscript and approving it for publication was Guido Lombardi.

is efficient concerning the computation of the Green matrix needed for FEM-BEM coupling [8]; (iii) an Adaptive Integration Technique (AIT) for the computation of the plasma source term has been implemented, to treat the problem of mismatching between plasma domain, whose boundary is not known a priori, and the mesh elements.

The resulting FRIDA-TD is based on an implicit time-stepping scheme to self-consistently and accurately solve the problem, providing a fast and flexible tool suitable for engineering-oriented purposes, such as the design of tokamak devices, set up of plasma operations, prediction of performance scenarios, and design of feedback control systems.

The paper is organized as follows. Section II reports preliminary considerations on the formulation of both the Free-Boundary Plasma Equilibrium Problem (FB-PEP) and the eddy current problem. The static version of the FRIDA code is also presented. In Sect. III the self-consistent coupling of FB-PEP and eddy current problem via implicit time-stepping scheme is presented. Section IV reports a detailed validation of FRIDA-TD, at first with the CarMa0NL code, and then against experimental data of the RFX-mod device. Finally, Sect. V is devoted to the conclusions and foreseen further developments.

II. PRELIMINARY CONSIDERATIONS ON THE FORMULATIONS OF THE PROBLEM

In the evolutionary equilibrium limit, the evolution of an axisymmetric plasma in presence of conducting structures surrounding the plasma itself is a time-dependent nonlinear problem. In the plasma domain, the governing equation is the Grad-Shafranov equation, which describes the problem of equilibrium of an axi-symmetric plasma in a suitable configuration of the external magnetic field. On the other hand, the problem of eddy currents, which are induced inside the conducting structures surrounding the plasma by time-varying magnetic fields, are described by Maxwell's equation in the magneto-quasistatic limit.

This is a coupled problem: on one hand, the time variation of the plasma equilibrium (e.g. variation of the total plasma current, of the internal profiles, of the plasma cross-section) would induce eddy currents in the passive structures; on the other hand, such current would themselves affect the plasma equilibrium.

Before going on, it is necessary to introduce and describe in detail the formulations of these two problems. Such formulations will be combined together in a coupled manner, as described in Sect. III.

A. FREE-BOUNDARY PLASMA EQUILIBRIUM PROBLEM

1) MATHEMATICAL FORMULATION

In a cylindrical coordinate system (r, ϕ, z), let us consider the domain Ω_v, which is the vacuum region inside the first wall and allowed to the plasma. The computational boundary of Ω_v is labeled as $\partial\Omega$. Inside Ω_v, the region which is actually occupied by the plasma, i.e. the plasma cross-section, is labeled Ω_p. In addition to this, we define also the plasma separatrix Γ_p, which is the *plasma-vacuum interface*. These regions can be seen in blue in Fig. 1 for RFX-mod device [9].

The Free-Boundary Plasma Equilibrium Problem (FB-PEP) in axisymmetric geometry is described by the Grad-Shafranov Equation (GSE), together with suitable boundary conditions (BCs):

$$\nabla \cdot \left(\frac{1}{r}\nabla\psi(\vec{r})\right) = \begin{cases} -\mu_0 j_\phi(\vec{r}, \psi) & \text{if } \boldsymbol{r} \in \Omega_p \\ 0 & \text{elsewhere} \end{cases} \tag{1}$$

$$\psi(\vec{r})\big|_{\partial\Omega} = \hat{\psi}_p(\vec{r}, \psi) + \hat{\psi}_{ext}(\vec{r}) \tag{2}$$

where μ_0 is the magnetic permeability of vacuum, and $\psi(\vec{r})$ is the poloidal magnetic flux *per radian* [10] (i.e. providing the poloidal magnetic field as $\frac{\nabla\psi}{r} \times \vec{e}_\phi$, $\vec{e}_\phi$ unit vector in ϕ direction), and $\hat{\psi}_p(\vec{r}, \psi)$ and $\hat{\psi}_{ext}(\vec{r})$ are the boundary conditions of the plasma and the external environment, respectively.

The current density in the Right Hand Side (RHS) of Eq. (1) can be described in the following ways:

$$\begin{aligned} j_\phi &= \lambda g(\psi, \psi_a, \psi_b) \\ &= \begin{cases} \lambda\left(r\dfrac{dp(\bar{\psi})}{d\bar{\psi}} + \dfrac{f(\bar{\psi})}{\mu_0 r}\dfrac{df(\bar{\psi})}{d\bar{\psi}}\right) \\ \lambda\left(\dfrac{r\beta_0}{R_0} + \dfrac{(1-\beta_0)R_0}{r}\right)(1-\bar{\psi}^{\alpha_M})^{\alpha_N} \end{cases} \end{aligned} \tag{3}$$

where the scaling parameter λ is needed to impose the total plasma current. Equations (3) mean that current density function $g(\psi, \psi_a, \psi_b)$ if described in terms of the profiles of the pressure $p(\bar{\psi})$ and the poloidal current function $f(\bar{\psi})$ [10], or through a suitable parametrization [11], [12] (here $[\alpha_M, \alpha_N, \beta_0]$ are the parameters, and R_0 is the machine major radius). In both cases, the normalized poloidal flux $\bar{\psi} = (\psi - \psi_a)/(\psi_b - \psi_a)$ is involved, where ψ_a and ψ_b are respectively the value of the flux at the magnetic axis and at the plasma separatrix Γ_p.

Information on the internal profiles, via $p(\bar{\psi})$ and $f(\bar{\psi})$ function or via the parametrization coefficients $[\alpha_M, \alpha_N, \beta_0]$, cannot be derived from the simple toroidal force balance, and must be determined either from experimental data, or from transport calculation [11], [12].

It is well known that the problem defined by Eqs. (1) - (2), with source term (3), is a *nonlinear* problem. The nonlinearity is due to the fact that (i) the source term depends on the solution $\psi(\boldsymbol{r})$ (Eq. (3)), (ii) the BCs depend also on the solution (Eq. (2)), and the plasma separatrix Γ_p, necessary to define the source domain Ω_p, is not known a priori, being itself an unknown of the problem, because it depends on the plasma equilibrium (i.e. *free-boundary* problem).

2) THE FRIDA CODE

In order to solve the FB-PEP in axisymmetric geometry, the FRIDA (FRee-boundary Integro-Differential

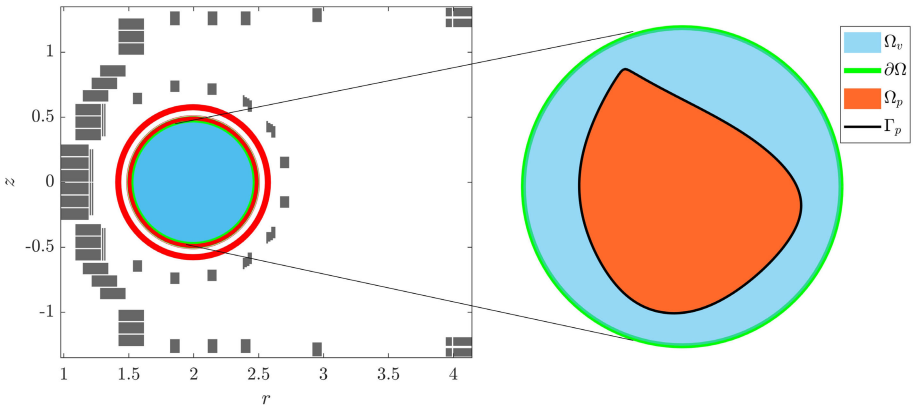

FIGURE 1. Domain regions for the case of RFX-mod device.

Axi-symmetric) code has been recently developed [8]. The proposed method is based on a novel Finite Element Method - Boundary Element Method (FEM-BEM) scheme, obtained from an improvement of the Hagenow-Lackner (HL) coupling method [13], and is able to efficiently model the equilibrium problem in unbounded domains by discretizing only the plasma region. As pointed out in detail in [8], the FRIDA code has several advantages. At first, it overcomes the convergence limitations of the original HL scheme, providing a FEM-BEM coupling scheme that has an optimal convergence rate. In addition to this, the computation of the Green matrix needed for FEM-BEM coupling, which depends only on the geometry of the domain triangulation, is performed beforehand during a preprocessing phase and it does not need to be repeated if another equilibrium with the same mesh is considered. Finally, an Adaptive Integration Technique (AIT) for the computation of the plasma source term has been implemented, to treat the mismatching problem between plasma separatrix, which is not known a priori, and the mesh elements.

In the FRIDA code, the discrete version of the FB-PEP equations is written as follows:

$$\begin{bmatrix} \boldsymbol{K} & \boldsymbol{K}_{bc} & 0 & 0 & -\mu_0 \boldsymbol{g}_p(\boldsymbol{x}) \\ 0 & \boldsymbol{E_I} & 0 & 0 & -\boldsymbol{G}_{bp}\boldsymbol{g}_p(\boldsymbol{x}) \\ \boldsymbol{\chi}_a(\boldsymbol{x}) & 0 & -1 & 0 & 0 \\ \boldsymbol{\chi}_b(\boldsymbol{x}) & 0 & 0 & -1 & 0 \\ 0 & 0 & 0 & 0 & I_t(\boldsymbol{x}) \end{bmatrix} \begin{bmatrix} \boldsymbol{\psi} \\ \hat{\boldsymbol{\psi}} \\ \psi_a \\ \psi_b \\ \lambda \end{bmatrix} = \begin{bmatrix} \boldsymbol{0} \\ \hat{\boldsymbol{\psi}}_{ext} \\ 0 \\ 0 \\ I_p \end{bmatrix} \tag{4}$$

where $\boldsymbol{x} = [\boldsymbol{\psi}, \hat{\boldsymbol{\psi}}, \psi_a, \psi_b, \lambda]^T$ is the vector of unknowns, $\boldsymbol{E_I}$ is the identity matrix, $\boldsymbol{K}$ and $\boldsymbol{K}_{bc}$ are the stiffness matrix related to the internal and boundary nodes. Please see eqs. 4.13 - 4.18 in [8] for a detailed description of the quantities.

Equation (4) can be written, by noting that $\lambda \boldsymbol{g}_p(\boldsymbol{x}) = \frac{1}{\mu_0}(\boldsymbol{K}\psi + \boldsymbol{K}_{bc}\hat{\psi})$, as:

$$\underbrace{\begin{bmatrix} \boldsymbol{K} & \boldsymbol{K}_{bc} & 0 & 0 & -\mu_0 \boldsymbol{g}_p(\boldsymbol{x}) \\ \hat{\boldsymbol{K}} & \hat{\boldsymbol{K}}_{bc} & 0 & 0 & 0 \\ \boldsymbol{\chi}_a(\boldsymbol{x}) & 0 & -1 & 0 & 0 \\ \boldsymbol{\chi}_b(\boldsymbol{x}) & 0 & 0 & -1 & 0 \\ 0 & 0 & 0 & 0 & I_t(\boldsymbol{x}) \end{bmatrix}}_{\boldsymbol{A}(\boldsymbol{x})} \underbrace{\begin{bmatrix} \boldsymbol{\psi} \\ \hat{\boldsymbol{\psi}} \\ \psi_a \\ \psi_b \\ \lambda \end{bmatrix}}_{\boldsymbol{x}} = \underbrace{\begin{bmatrix} \boldsymbol{0} \\ \hat{\boldsymbol{\psi}}_{ext} \\ 0 \\ 0 \\ I_p \end{bmatrix}}_{\boldsymbol{b}} \tag{5}$$

Equation (5), which can be written more compactly as $\boldsymbol{F}(\boldsymbol{x}) = \boldsymbol{A}(\boldsymbol{x})\boldsymbol{x} - \boldsymbol{b} = 0$, is a nonlinear system of equations of dimension $(N_n+3)\times(N_n+3)$, where N_n is the number of mesh nodes of the triangular mesh of Ω_v, considering both internal and boundary nodes. The solution of (5) gives the poloidal flux ψ on the entire computational domain Ω_v, included its boundary $\partial\Omega$, the values of the flux at both the magnetic axis and separatrix (i.e. ψ_a, ψ_b), as well as the scaling parameter λ of the total plasma current.

The solution of this system, provided a suitable initial guess $\boldsymbol{x}_0$ is obtained, in the FRIDA code, exploiting Newton-like algorithms, such as Newton-Raphson or Newton-Krylov [14]. In [8], a detailed comparison of these two methods is also reported.

3) BOUNDARY CONDITIONS

In the previous formulation, Ω_v is chosen such as the only source term inside the computational domain is due to the plasma current density (FEM-BEM formulation), while all the other sources (i.e. active coils for static equilibria) are taken into account through the BCs term $\hat{\boldsymbol{\psi}}_{ext}$ in Eq. (2) (integral formulation).

For transient problems, in which eddy currents have to be also considered, the term $\hat{\psi}_{ext}$ must account also for their contribution. Equation (2) is then modified as follows:

$$\psi(\vec{r})\big|_{\partial\Omega} = \hat{\psi}_p(\vec{r},\psi) + \hat{\psi}_a(\vec{r}) + \hat{\psi}_c(\vec{r},\psi) \tag{6}$$

where $\hat{\psi}_a(\vec{r})$ is the contribution of the active coils, and $\hat{\psi}_c(\vec{r},\psi)$ of the passive conductors. Since, as already mentioned at the beginning of this section, the eddy current evolution is affected by the plasma itself, also their contribution to the boundary condition depends on the plasma, giving another source of nonlinearity.

It is worth noting that, depending on the formulation, the active coils can be modeled as voltage-fed (V-fed) or current-fed (I-fed) conductors. In the former case, both active and passive conductors in Eq. (6) are considered through the term $\hat{\psi}_c(\vec{r},\psi)$. In the following sections, both these formulations will be considered.

The vector $\hat{\boldsymbol{\psi}}_c$, which is the discrete counterpart of $\hat{\psi}_c(\vec{r},\psi)$, gives additional Degrees of Freedom (DoFs). Thus, the second equation of (5) has to be modified accordingly:

$$\hat{\boldsymbol{K}}\boldsymbol{\psi} + \hat{\boldsymbol{K}}_{bc}\hat{\boldsymbol{\psi}} = \hat{\boldsymbol{\psi}}_a + \hat{\boldsymbol{\psi}}_c \tag{7}$$

In principle, the vector of DoF $\boldsymbol{x}$ should now include also $\hat{\boldsymbol{\psi}}_c$, leading to a larger system of equations. We will show how this can be avoided, keeping $\hat{\boldsymbol{\psi}}_c$ into account implicitly without adding DOFs to the original ones.

B. EDDY-CURRENT PROBLEM

For the eddy current problem in axisymmetric geometry, we consider at first the weak formulation of Ohm's law:

$$\int_{V_c} \vec{w}\left(\eta\vec{J} - \vec{E}\right)dV = 0 \tag{8}$$

where $\vec{w}$ is a test function, the vector field $\vec{J}$ and $\vec{E}$ are respectively the current density and the electric fields in the conducting domain V_c, and η is the electric resistivity. Figure 2 shows, for RFX-mod, the conducting domain V_c in the poloidal plane (red), the coils (gray), the domain Ω_v available to the plasma (blue), and its boundary $\partial\Omega$ (green).

Exploiting the axial-symmetry, since $\vec{J} = (0, J_\varphi, 0)$ and $\vec{E} = (0, E_\varphi, 0)$:

$$\int_0^{2\pi} d\varphi \int_{\Omega_c} r\vec{w}\left(\eta J_\varphi - E_\varphi\right)d\Omega = 0 \tag{9}$$

where Ω_c is the projection of V_c in the poloidal plane. The electric field is expressed in terms of the magnetic vector potential $\vec{A}$ and the scalar electric potential ϕ ($E_\varphi = -\frac{\partial A_\varphi}{\partial t} - \nabla\phi$), and we use the Biot-Savart integral :

$$A_\varphi(\vec{r},t) = \frac{\mu_0}{4\pi}\int_{V_c}\frac{J_\varphi(\vec{r}',t)}{|\vec{r}-\vec{r}'|}dV' + A_{s\varphi}(\vec{r},\bar{\psi},t) \tag{10}$$

where[1] $\vec{A}_s(\vec{r},t)$ is the magnetic vector potential given by sources external to the conducting structures, such as the plasma and the active conductors in case of I-fed formulation. It follows that:

$$\int_{\Omega_c} 2\pi rw\left\{\eta J_\varphi + \frac{\partial}{\partial t}\left[\frac{\mu_0}{4\pi}\int_{V_c}\frac{J(\vec{r}',t)}{|\vec{r}-\vec{r}'|}dV' + A_s(\vec{r},t)\right]\right\}d\Omega = 0 \tag{11}$$

Following the standard FEM approach, the computational domain is discretized in triangular elements [15]. In addition to this, we follow the Galerkin approach, choosing as test functions $w(\vec{r})$ polynomials of degree N_d defined as:

$$w(\vec{r}) = \sum_{i=0}^{N_d}\sum_{j=0}^{N_d} a_{ij} r^i z^j \tag{12}$$

where a_{hk} are the coefficients of the basis functions. In this context, we considered polynomial up to degree $N_d = 3$, in order to model accurately the skin effect occurring in the passive structures, especially during fast transients.

By expanding J_φ in terms of basis functions (12), we can write (11) as:

$$\boldsymbol{L}\frac{d\boldsymbol{j}_c}{dt} + \boldsymbol{R}\boldsymbol{j}_c = -\boldsymbol{M}\frac{d\boldsymbol{i}_s}{dt} \tag{13}$$

where $\boldsymbol{j}_c$ is the discrete counterpart of J_φ, $\boldsymbol{i}_s$ is the vector of external currents (i.e. active currents $\boldsymbol{i}_a$ for I-FED approach, and plasma nodal currents $\boldsymbol{i}_p(\bar{\psi})$), and:

$$L_{ij} = \int_{\Omega_c} 2\pi rw_i(\vec{r})\left[\frac{\mu_0}{4\pi}\int_{V_c}\frac{w_j(\vec{r}')}{|\vec{r}-\vec{r}'|}dV'\right]d\Omega \tag{14}$$

$$R_{ij} = \int_{\Omega_c} 2\pi r\eta w_i(\vec{r})w_j(\vec{r})d\Omega \tag{15}$$

$$M_{s,ij} = \int_{\Omega_c} 2\pi rw_i(\vec{r})\left[\frac{\mu_0}{4\pi}\int_{V_{s_i}}\frac{\chi_{s_i}(\vec{r}')}{|\vec{r}-\vec{r}'|}dV'\right]d\Omega \tag{16}$$

where V_{s_i} defines the domain of *ith* external source and $\chi_{s_i}(\vec{r}')$ is a suitable basis function defined on V_{s_i}. For a more detailed description see appendix.

By introducing the quantity $\boldsymbol{a}$ such as $\boldsymbol{a} = \boldsymbol{U}\vec{A}_\varphi$, where the matrix $\boldsymbol{U}$ is defined in Eq. (75), and by considering that:

$$\boldsymbol{a} = \boldsymbol{a}_c + \boldsymbol{a}_s = \boldsymbol{L}\boldsymbol{j}_c + \boldsymbol{M}\boldsymbol{i}_s \tag{17}$$

$$\Rightarrow \boldsymbol{j}_c = \boldsymbol{L}^{-1}(\boldsymbol{a} - \boldsymbol{M}\boldsymbol{i}_s) \tag{18}$$

equation (13) is written to obtain the well-known state space form:

$$\frac{d\boldsymbol{a}}{dt} = -\boldsymbol{R}\boldsymbol{L}^{-1}\boldsymbol{a} + \boldsymbol{R}\boldsymbol{L}^{-1}\boldsymbol{M}\boldsymbol{i}_{eq} \tag{19}$$

which gives the *current fed formulation* of the eddy current problem.

On the other hand, the active coils can be modeled as passive conductors fed by a source voltage rather than by a prescribed set of currents. However, not all the external sources can be written with a V-fed approach, i.e. the plasma

[1] Since we are considering the φ components of the quantities, in the following part of the discussion the subscript φ will be dropped, and the components will be specified only if necessary.

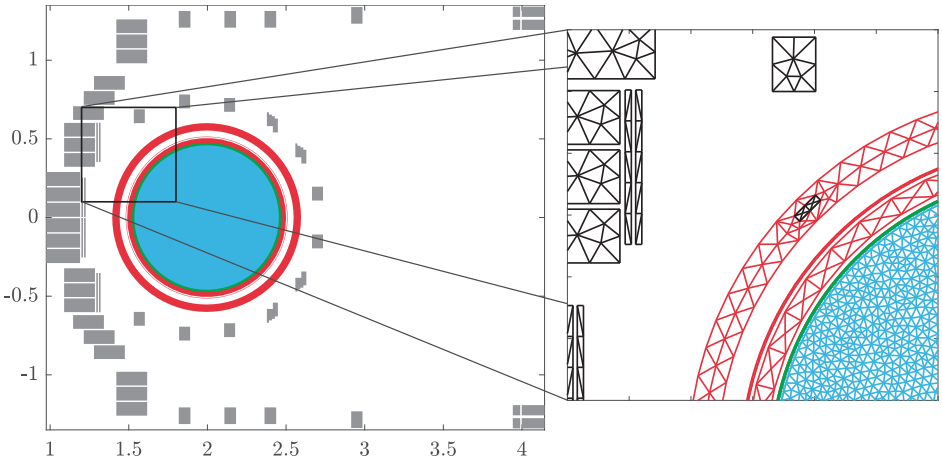

FIGURE 2. Definition of regions for RFX-mod case: conducting domain Ω_c in the poloidal plane (red), the coils (gray), the domain Ω_v available to the plasma (blue), and its boundary $\partial\Omega$ (green).

currents have still to be written following an I-fed formulation. For this reason, we will refer in the following to the *voltage-current fed formulation* (VI-fed):

$$\boldsymbol{L}\frac{d\boldsymbol{j}_c}{dt} + \boldsymbol{R}\boldsymbol{j}_c = -\boldsymbol{M}\frac{d\boldsymbol{i}_s}{dt} + \boldsymbol{V}\boldsymbol{D}\boldsymbol{v} \tag{20}$$

where $\boldsymbol{D}$ is an incidence matrix related to the nodes belonging to the electrodes, $\boldsymbol{V}$ is defined in (74) and $\boldsymbol{v}$ is the vector of applied voltages. It follows that:

$$\frac{d\boldsymbol{a}}{dt} = -\boldsymbol{R}\boldsymbol{L}^{-1}\boldsymbol{a} + \boldsymbol{R}\boldsymbol{L}^{-1}\boldsymbol{M}\boldsymbol{i}_s + \boldsymbol{V}\boldsymbol{D}\boldsymbol{v} \tag{21}$$

1) MODEL OF TOROIDALLY DISCONTINUOUS STRUCTURES

We consider, at this point, the case of *toroidally discontinuous* conducting structures. Discontinuous conducting structures can be found in some experimental devices in order to allow, through insulated gaps, the penetration of the electric and magnetic fields into the plasma region [16]. This problem has been already studied for eddy currents in the filamentary approximation [17], but, it has been never developed for a general Galerkin-based integral approach on triangular meshes.

In the case of toroidally closed conducting structures, Eq. (13) holds because the passive structures are short-circuited, this is no longer true for toroidally discontinuous structures. This fact is briefly summarized in Figs. 3. Indeed, if the conducting structures are toroidally not continuous, a voltage applied to the points P and Q develops in the case of transient magneto-quasistatic phenomena, as can be seen in fig. 3. In such case, Eq. (13) becomes:

$$\boldsymbol{L}\frac{d\boldsymbol{j}_c}{dt} + \boldsymbol{R}\boldsymbol{j}_c = -\boldsymbol{M}\frac{d\boldsymbol{i}_s}{dt} + \boldsymbol{V}v_{gap} \tag{22}$$

with an additional degree of freedom v_{gap} for every toroidally discontinuous structure. The matrix $\boldsymbol{V}$ is defined as 74.

In order to close the system, adding additional constrains have to be considered. This means to impose, for every toroidally open structure, that the total induced current which flows through the poloidal plane has to be zero. Thus, for each structure:

$$\int_{\Omega_c} J_\varphi(\vec{r})d\Omega = 0 \Leftrightarrow \boldsymbol{\alpha}^T\boldsymbol{j}_c = 0 \tag{23}$$

where

$$\alpha_i = \sum_{j=1}^{N_j^i}\int_{\Omega_j} w_{ij}(\vec{r})d\Omega \tag{24}$$

where Ω_i is the local support given by the N_j^i triangles sharing the *ith* node.

By combining (18) with (23) we obtain the additional constrain to close the system:

$$\boldsymbol{\alpha}^T\boldsymbol{j}_c = \underbrace{\boldsymbol{\alpha}^T\boldsymbol{L}^{-1}}_{\boldsymbol{\beta}^T}\boldsymbol{a} - \underbrace{\boldsymbol{\alpha}^T\boldsymbol{L}^{-1}\boldsymbol{M}_s}_{\boldsymbol{H}}\boldsymbol{i}_s = 0 \tag{25}$$

The state-space equation (19) then becomes:

$$\underbrace{\begin{bmatrix}\boldsymbol{E_I} & \boldsymbol{0}\\ \boldsymbol{0} & 0\end{bmatrix}}_{\boldsymbol{E}}\frac{\partial}{\partial t}\underbrace{\begin{bmatrix}\boldsymbol{a}\\ v_{gap}\end{bmatrix}}_{\boldsymbol{y}} = \underbrace{\begin{bmatrix}-\boldsymbol{R}\boldsymbol{L}^{-1} & \boldsymbol{V}\\ \boldsymbol{\beta}^T & 0\end{bmatrix}}_{\boldsymbol{A}}\begin{bmatrix}\boldsymbol{a}\\ v_{gap}\end{bmatrix} + \underbrace{\begin{bmatrix}\boldsymbol{R}\boldsymbol{L}^{-1}\boldsymbol{M}\\ -\boldsymbol{H}\end{bmatrix}}_{\boldsymbol{B}}\boldsymbol{i}_s \tag{26}$$

where $\boldsymbol{E_I}$ is the identity matrix and $\boldsymbol{V}$ is defined in (74). In case of N_{open} toroidally discontinuous structures, (25) has to be imposed for each structure. In this case, $\boldsymbol{v}_{gap}$ is a vector of dimension N_{open}, and $\boldsymbol{\alpha}$ and $\boldsymbol{\beta}^T$ are matrices with N_{open} rows.

Concerning the VI-fed formulation, (22) can be written as:

$$\frac{d\boldsymbol{a}}{dt} = -\boldsymbol{R}\boldsymbol{L}^{-1}\boldsymbol{a} + \boldsymbol{R}\boldsymbol{L}^{-1}\boldsymbol{M}\boldsymbol{i}_s + \boldsymbol{V}\boldsymbol{D}\boldsymbol{v} + \boldsymbol{V}v_{gap} \tag{27}$$

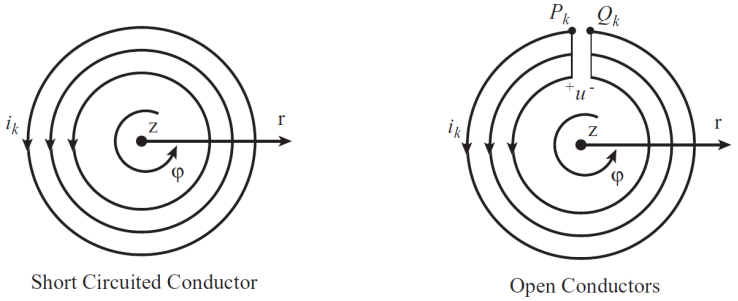

FIGURE 3. Toroidally continuous (left) and discontinuous structures (right).

which can be written as:

$$\underbrace{\begin{bmatrix} \boldsymbol{E_I} & \boldsymbol{0} \\ \boldsymbol{0} & 0 \end{bmatrix}}_{\boldsymbol{E}} \frac{\partial}{\partial t} \underbrace{\begin{bmatrix} \boldsymbol{a} \\ v_{gap} \end{bmatrix}}_{\boldsymbol{y}} = \underbrace{\begin{bmatrix} -\boldsymbol{R}\boldsymbol{L}^{-1} & \boldsymbol{V} \\ \vec{\beta}^T & 0 \end{bmatrix}}_{\boldsymbol{A}} \begin{bmatrix} \boldsymbol{a} \\ v_{gap} \end{bmatrix} + \underbrace{\begin{bmatrix} \boldsymbol{R}\boldsymbol{L}^{-1}\boldsymbol{M} \\ -\boldsymbol{H} \end{bmatrix}}_{\boldsymbol{B}_i} \boldsymbol{i}_s + \underbrace{\begin{bmatrix} \boldsymbol{V}\boldsymbol{D} \\ 0 \end{bmatrix}}_{\boldsymbol{B}_v} \boldsymbol{v} \tag{28}$$

In case of N_{open} toroidally discontinuous structures, the same considerations made for the I-fed formulation holds.

It is important to note than (28) is formally equivalent to (26), by defining accordingly $\boldsymbol{E}, \boldsymbol{y}, \boldsymbol{A}, \boldsymbol{B}$.

III. SELF-CONSISTENT COUPLING OF FB-PEP AND EDDY CURRENT PROBLEM VIA FULLY IMPLICIT TIME-STEPPING SCHEME

A. MATHEMATICAL FORMULATION

The self-consistent coupling between free-boundary plasma equilibrium and eddy current models is performed by introducing the so-called coupling surface S_e. A proper coupling surface is chosen such as it does not intersect either the plasma or the passive structures, and all the conducting structures are placed outside it. This approach is very common in the fusion community for those applications dealing with coupling/decoupling problems [7], [18], [19]. A sketched view of this configuration can be seen in Fig. 4, where the trace Γ_{eq} of the coupling surface in the poloidal plane is shown, together with the other domains.

An equivalent current $\boldsymbol{i}_{eq}$ flows on the coupling surface, and produces, outside it, the same magnetic flux of the plasma. The procedure for the computation of $\boldsymbol{i}_{eq}$, given the actual vector of plasma nodal currents, is explained in App. . The matrix $\boldsymbol{M}$ is then computed considering the mutual coupling between the passive conductors and the N_{eq} circuits on the coupling surface via (16).

Let us consider the general case of Eq. (26), together with Eq. (18), and writing explicitly the source terms due to active coils and plasma. In case of toroidally continuous structures, Eq. (19) can be derived straightforwardly from Eq. (26). We obtain the following system Differential

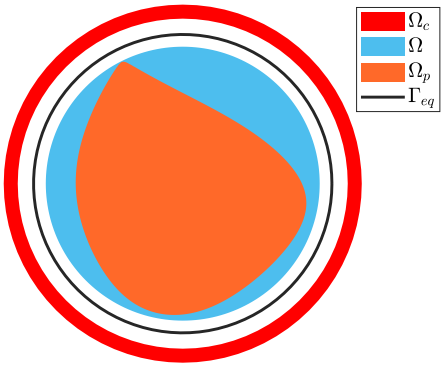

FIGURE 4. Sketched view of the geometry for the coupling of FB-PEP and eddy current problem.

Algebraic Equations (DAE):

$$\begin{cases} \boldsymbol{E}\dot{\boldsymbol{y}} = \boldsymbol{A}\boldsymbol{y} + \boldsymbol{B}_a\boldsymbol{u}_a + \boldsymbol{B}_p\lambda\boldsymbol{g}_p(\boldsymbol{x}) \\ \boldsymbol{j}_c = \boldsymbol{C}\boldsymbol{y} + \boldsymbol{D}_a\boldsymbol{u}_a + \boldsymbol{D}_p\lambda\boldsymbol{g}_p(\boldsymbol{x}) \end{cases} \tag{29}$$

Matrices $\boldsymbol{E}$, $\boldsymbol{y}$, $\boldsymbol{A}$ have been defined in (26) (I-fed) or (28) (VI-fed). The definition of $\boldsymbol{B}_p$, $\boldsymbol{C}$, and $\boldsymbol{D}_p$ are the same for I-fed and VI-fed cases:

$$\boldsymbol{B}_p = \begin{bmatrix} \boldsymbol{R}\boldsymbol{L}^{-1}\boldsymbol{M}_{cp}\boldsymbol{T}_{eq} \\ -\boldsymbol{H}_p \end{bmatrix} \tag{30}$$

$$\boldsymbol{C} = \begin{bmatrix} \boldsymbol{L}^{-1} & \boldsymbol{0} \end{bmatrix} \tag{31}$$

$$\boldsymbol{D}_p = -\boldsymbol{L}^{-1}\boldsymbol{M}_{cp}\boldsymbol{T}_{eq} \tag{32}$$

where $\boldsymbol{M}_{cp}$ is the mutual inductance matrix between equivalent plasma currents and the passive structures, defined in (16), and $\boldsymbol{T}_{eq}$ is a $N_{eq} \times N_n$ matrix giving the equivalent current $\boldsymbol{i}_{eq}$ from the plasma nodal currents $\boldsymbol{i}_p$ defined in App. . Conversely, the definition of $\boldsymbol{B}_a$ and $\boldsymbol{D}_a$ depends on the formulation:

$$\boldsymbol{B}_a = \begin{bmatrix} \boldsymbol{R}\boldsymbol{L}^{-1}\boldsymbol{M}_{ca} \\ -\boldsymbol{H}_a \end{bmatrix} \quad \boldsymbol{D}_a = -\boldsymbol{L}^{-1}\boldsymbol{M}_{ca} \quad \text{I-fed} \tag{33}$$

$$\boldsymbol{B}_a = \begin{bmatrix} \boldsymbol{V}\boldsymbol{D} \\ 0 \end{bmatrix} \quad \boldsymbol{D}_a = \boldsymbol{0} \quad \text{VI-fed} \tag{34}$$

where $\boldsymbol{M}_{ca}$ is the mutual inductance matrix between active conductors and the passive structures, also defined in (16).

The full system of equations of the coupled problem follows:

$$\boldsymbol{E}\dot{\boldsymbol{y}} = \boldsymbol{A}\boldsymbol{y} + \boldsymbol{B}_a\boldsymbol{u}_a + \boldsymbol{B}_p\lambda\boldsymbol{g}_p(\boldsymbol{x}) \quad (35)$$

$$\boldsymbol{j}_c = \boldsymbol{C}\boldsymbol{y} + \boldsymbol{D}_a\boldsymbol{u}_a + \boldsymbol{D}_p\lambda\boldsymbol{g}_p(\boldsymbol{x}) \quad (36)$$

$$\hat{\boldsymbol{\psi}}_c = \tilde{\boldsymbol{G}}_{bc}\boldsymbol{j}_c \quad (37)$$

$$\boldsymbol{K}\boldsymbol{\psi} + \boldsymbol{K}_{bc}\hat{\boldsymbol{\psi}} - \mu_0\lambda\boldsymbol{g}_p(\boldsymbol{x}) = \boldsymbol{0} \quad (38)$$

$$\hat{\boldsymbol{K}}\boldsymbol{\psi} + \hat{\boldsymbol{K}}_{bc}\hat{\boldsymbol{\psi}} - \hat{\boldsymbol{\psi}}_c - \hat{\boldsymbol{\psi}}_a = \boldsymbol{0} \quad (39)$$

$$\boldsymbol{\chi}_a(\boldsymbol{x})\boldsymbol{\psi} - \psi_a = 0 \quad (40)$$

$$\boldsymbol{\chi}_b(\boldsymbol{x})\boldsymbol{\psi} - \psi_b = 0 \quad (41)$$

$$\lambda I_t(\boldsymbol{x}) - I_p = 0 \quad (42)$$

consisting in 8 equations, 5 vectorial plus 3 scalar equations. The system describes a time-dependent nonlinear problem: the plasma contribution enters the eddy current problem trough terms $\boldsymbol{B}_p\lambda\boldsymbol{g}_p(\boldsymbol{x})$ and $\boldsymbol{D}_p\lambda\boldsymbol{g}_p(\boldsymbol{x})$ of (29), whereas the eddy current contribution enters the FB-PEP trough the term $\hat{\boldsymbol{\psi}}_c$ of Eq. (39), which is the BCs of the FB-PEP due to the eddy currents. Such term is computed via the Green matrix $\tilde{\boldsymbol{G}}_{bc}$, defined in (76).

The DAE problem (35) is solved via Crank-Nicolson method, giving:

$$\boldsymbol{E}\left(\boldsymbol{y}^{h+1} - \boldsymbol{y}^h\right) = \frac{\Delta t}{2}\left[f(t^h, \boldsymbol{x}^h, \boldsymbol{y}^h) + f(t^{h+1}, \boldsymbol{x}^{h+1}, \boldsymbol{y}^{h+1})\right] \quad (43)$$

where $f(t, \boldsymbol{x}, \boldsymbol{y}) = \boldsymbol{A}\boldsymbol{y} + \boldsymbol{B}_a\boldsymbol{u}_a + \boldsymbol{B}_p\lambda\boldsymbol{g}_p(\boldsymbol{x})$, h stands for the time instant. The RHS of (43) can be written as (note that $\boldsymbol{I}_p$ is written in place of $\lambda\boldsymbol{g}_p(\boldsymbol{x})$):

$$\begin{aligned}\boldsymbol{E}\left(\boldsymbol{y}^{h+1} - \boldsymbol{y}^h\right) = \frac{\Delta t}{2}\big(&\boldsymbol{A}\boldsymbol{y}^h + \boldsymbol{B}_a\boldsymbol{x}_a^h \\ &+ \boldsymbol{B}_p\boldsymbol{I}_p^h + \boldsymbol{A}\boldsymbol{y}^{h+1} + \boldsymbol{B}_a\boldsymbol{u}_a^{h+1} + \boldsymbol{B}_p\boldsymbol{I}_p^{h+1}\big)\end{aligned} \quad (44)$$

after some manipulations, we obtain:

$$\begin{aligned}&\underbrace{\left(\boldsymbol{E} - \frac{\Delta t}{2}\boldsymbol{A}\right)}_{\boldsymbol{A}_1}\boldsymbol{y}^{h+1} - \frac{\Delta t}{2}\boldsymbol{B}_p\boldsymbol{I}_p^{h+1} \\ &= \underbrace{\left(\boldsymbol{E} + \frac{\Delta t}{2}\boldsymbol{A}\right)}_{\boldsymbol{A}_2}\boldsymbol{y}^h + \frac{\Delta t}{2}\left(\boldsymbol{B}_a\boldsymbol{u}_a^h + \boldsymbol{B}_p\boldsymbol{I}_p^h + \boldsymbol{B}_a\boldsymbol{u}_a^{h+1}\right)\end{aligned} \quad (45)$$

We exploit now the relation $(\lambda\boldsymbol{g}_p(\boldsymbol{x}))^{h+1} = \frac{1}{\mu_0}(\boldsymbol{K}\boldsymbol{\psi}^{h+1} + \boldsymbol{K}_{bc}\hat{\boldsymbol{\psi}}^{h+1})$, as done in [8]:

$$\boldsymbol{A}_1\boldsymbol{y}^{h+1} - \frac{\Delta t}{2}\boldsymbol{B}_p\frac{1}{\mu_0}(\boldsymbol{K}\boldsymbol{\psi}^{h+1} + \boldsymbol{K}_{bc}\hat{\boldsymbol{\psi}}^{h+1}) \quad (46)$$

$$= \boldsymbol{A}_2\boldsymbol{y}^h + \frac{\Delta t}{2}\left(\boldsymbol{B}_a\boldsymbol{u}_a^h + \boldsymbol{B}_p\boldsymbol{I}_p^h + \boldsymbol{B}_a\boldsymbol{u}_a^{h+1}\right) \quad (47)$$

which can be written as:

$$\begin{aligned}&\boldsymbol{y}^{h+1} - \frac{\Delta t}{2\mu_0}\boldsymbol{A}_1^{-1}\boldsymbol{B}_p\boldsymbol{K}\boldsymbol{\psi}^{h+1} - \frac{\Delta t}{2\mu_0}\boldsymbol{A}_1^{-1}\boldsymbol{B}_p\boldsymbol{K}_{bc}\hat{\boldsymbol{\psi}}^{h+1} \\ &= \boldsymbol{A}_1^{-1}\boldsymbol{A}_2\boldsymbol{y}^h + \frac{\Delta t}{2}\boldsymbol{A}_1^{-1}\left(\boldsymbol{B}_a\boldsymbol{u}_a^h + \boldsymbol{B}_p\boldsymbol{I}_p^h + \boldsymbol{B}_a\boldsymbol{u}_a^{h+1}\right)\end{aligned} \quad (48)$$

or more compactly as:

$$\boldsymbol{y}^{h+1} - \hat{\boldsymbol{Q}}\boldsymbol{\psi}^{h+1} - \hat{\boldsymbol{Q}}_{bc}\hat{\boldsymbol{\psi}}^{h+1} = \boldsymbol{b}_{\boldsymbol{y}} \quad (49)$$

where the following quantities have been defined:

$$\hat{\boldsymbol{Q}} = \frac{\Delta t}{2\mu_0}\boldsymbol{A}_1^{-1}\boldsymbol{B}_p\boldsymbol{K} \quad (50)$$

$$\hat{\boldsymbol{Q}}_{bc} = \frac{\Delta t}{2\mu_0}\boldsymbol{A}_1^{-1}\boldsymbol{B}_p\hat{\boldsymbol{K}}_{bc} \quad (51)$$

$$\boldsymbol{b}_{\boldsymbol{y}} = \boldsymbol{A}_1^{-1}\boldsymbol{A}_2\boldsymbol{y}^h + \frac{\Delta t}{2}\boldsymbol{A}_1^{-1}\left(\boldsymbol{B}_a\boldsymbol{u}_a^h + \boldsymbol{B}_p\boldsymbol{I}_p^h + \boldsymbol{B}_a\boldsymbol{u}_a^{h+1}\right) \quad (52)$$

The passive currents density $\boldsymbol{j}_c$ is computed via (36), together with (49) and giving that $(\lambda\boldsymbol{g}_p(\boldsymbol{x}))^{h+1} = \frac{1}{\mu_0}(\boldsymbol{K}\boldsymbol{\psi}^{h+1} + \boldsymbol{K}_{bc}\hat{\boldsymbol{\psi}}^{h+1})$:

$$\boldsymbol{j}_c^{h+1} = \boldsymbol{C}\boldsymbol{y}^{h+1} + \boldsymbol{D}_a\boldsymbol{u}_a^{h+1} + \boldsymbol{D}_p\boldsymbol{I}_p^{h+1} \quad (53)$$

$$\begin{aligned}&= \boldsymbol{C}\left(\hat{\boldsymbol{Q}}\boldsymbol{\psi}^{h+1} + \hat{\boldsymbol{Q}}_{bc}\hat{\boldsymbol{\psi}}^{h+1} + \boldsymbol{b}_{\boldsymbol{x}}\right) + \boldsymbol{D}_a\boldsymbol{u}_a^{h+1} + \\ &\quad + \boldsymbol{D}_p\frac{1}{\mu_0}(\boldsymbol{K}\boldsymbol{\psi}^{h+1} + \boldsymbol{K}_{bc}\hat{\boldsymbol{\psi}}^{h+1})\end{aligned} \quad (54)$$

$$\begin{aligned}&= \left(\boldsymbol{C}\hat{\boldsymbol{Q}} + \frac{1}{\mu_0}\boldsymbol{D}_p\boldsymbol{K}\right)\boldsymbol{\psi}^{h+1} \\ &\quad + \left(\boldsymbol{C}\hat{\boldsymbol{Q}}_{bc} + \frac{1}{\mu_0}\boldsymbol{D}_p\boldsymbol{K}_{bc}\right)\hat{\boldsymbol{\psi}}^{h+1} + +\boldsymbol{C}\boldsymbol{b}_{\boldsymbol{x}} + \boldsymbol{D}_a\boldsymbol{u}_a^{h+1}\end{aligned} \quad (55)$$

The contribution of eddy currents to the BCs term $\hat{\boldsymbol{\psi}}_c$ is readily obtained through coupling equation (37):

$$\hat{\boldsymbol{\psi}}_c = \tilde{\boldsymbol{G}}_{bc}\boldsymbol{j}_c \quad (56)$$

$$= \tilde{\boldsymbol{G}}_{bc}\Bigg[\left(\boldsymbol{C}\hat{\boldsymbol{Q}} + \frac{1}{\mu_0}\boldsymbol{D}_p\boldsymbol{K}\right)\boldsymbol{\psi}^{h+1} + \quad (57)$$

$$+ \left(\boldsymbol{C}\hat{\boldsymbol{Q}}_{bc} + \frac{1}{\mu_0}\boldsymbol{D}_p\boldsymbol{K}_{bc}\right)\hat{\boldsymbol{\psi}}^{h+1} + \boldsymbol{C}\boldsymbol{b}_{\boldsymbol{x}} + \boldsymbol{D}_a\boldsymbol{u}_a^{h+1}\Bigg] \quad (58)$$

which is written as:

$$\hat{\boldsymbol{\psi}}_c + \hat{\boldsymbol{P}}\psi + \hat{\boldsymbol{P}}_{bc}\hat{\psi} = \boldsymbol{b}_{\hat{\psi}_c} \quad (59)$$

where:

$$\hat{\boldsymbol{P}} = -\tilde{\boldsymbol{G}}_{bc}\left(\boldsymbol{C}\hat{\boldsymbol{Q}} + \frac{1}{\mu_0}\boldsymbol{D}_p\boldsymbol{K}\right) \quad (60)$$

$$\hat{\boldsymbol{P}}_{bc} = -\tilde{\boldsymbol{G}}_{bc}\left(\boldsymbol{C}\hat{\boldsymbol{Q}}_{bc} + \frac{1}{\mu_0}\boldsymbol{D}_p\boldsymbol{K}_{bc}\right) \quad (61)$$

$$\boldsymbol{b}_{\hat{\psi}_c} = \tilde{\boldsymbol{G}}_{bc}\left[\boldsymbol{C}\boldsymbol{b}_{\boldsymbol{x}} + \boldsymbol{D}_a\boldsymbol{u}_a^{h+1}\right] \quad (62)$$

In principle, as already mentioned in Par. II-A3, the unknowns $\hat{\boldsymbol{\psi}}_c$ have to be added to the vector of DoFs. From the computational point of view, this could increase the computational cost to solve the problem, because equation (59) is fully populated. A convenient solution is to take into account implicitly of $\hat{\boldsymbol{\psi}}_c$, by including (59) into (39). Since $\hat{\boldsymbol{\psi}}_c = -\hat{\boldsymbol{P}}\psi - \hat{\boldsymbol{P}}_{bc}\hat{\psi} + \boldsymbol{b}_{\hat{\psi}_c}$, (39) becomes:

$$\left(\hat{\boldsymbol{K}} + \hat{\boldsymbol{P}}\right)\boldsymbol{\psi} + \left(\hat{\boldsymbol{K}}_{bc} + \hat{\boldsymbol{P}}_{bc}\right)\hat{\boldsymbol{\psi}} = \hat{\boldsymbol{\psi}}_a + \boldsymbol{b}_{\hat{\psi}_c} \quad (63)$$

which can be written more compactly:

$$\hat{\boldsymbol{S}}\boldsymbol{\psi} + \hat{\boldsymbol{S}}_{bc}\hat{\boldsymbol{\psi}} = \boldsymbol{b}_{\hat{\psi}} \tag{64}$$

where:

$$\hat{\boldsymbol{S}} = \hat{\boldsymbol{K}} + \hat{\boldsymbol{P}} \tag{65}$$

$$\hat{\boldsymbol{S}}_{bc} = \hat{\boldsymbol{K}}_{bc} + \hat{\boldsymbol{P}}_{bc} \tag{66}$$

$$\boldsymbol{b}_{\hat{\psi}} = \hat{\boldsymbol{\psi}}_a + \boldsymbol{b}_{\hat{\psi}_c} \tag{67}$$

Finally, the following system of equations, which is the discrete counterpart of Eqs. (35) - (42), can be written:

$$\underbrace{\begin{bmatrix} \boldsymbol{K} & \boldsymbol{K}_{bc} & 0 & 0 & -\mu_0 \boldsymbol{g}_p(\boldsymbol{x}) \\ \hat{\boldsymbol{S}} & \hat{\boldsymbol{S}}_{bc} & 0 & 0 & 0 \\ \boldsymbol{\chi}_a(\boldsymbol{x}) & 0 & -1 & 0 & 0 \\ \boldsymbol{\chi}_b(\boldsymbol{x}) & 0 & 0 & -1 & 0 \\ 0 & 0 & 0 & 0 & I_t(\boldsymbol{x}) \end{bmatrix}}_{\boldsymbol{A}(\boldsymbol{x}^h)} \underbrace{\begin{bmatrix} \boldsymbol{\psi} \\ \hat{\boldsymbol{\psi}} \\ \psi_a \\ \psi_b \\ \lambda \end{bmatrix}}_{\boldsymbol{x}^{h+1}} = \underbrace{\begin{bmatrix} 0 \\ \boldsymbol{b}_{\hat{\psi}} \\ 0 \\ 0 \\ I_p \end{bmatrix}}_{\boldsymbol{b}^h} \tag{68}$$

It is a vector-valued nonlinear problem of the form $\boldsymbol{F}(\boldsymbol{x}) = \boldsymbol{A}(\boldsymbol{x})\boldsymbol{x} - \boldsymbol{b} = \boldsymbol{0}$, that has to be solved at each time step h to find the new solution $\boldsymbol{x}^{h+1}$.

It is important to notice that the number of DoFs of (68) is the same as (5); moreover, it does not depend on the discretization of the passive conductors, meaning that the accuracy of the eddy current problem can be improved without affecting the overall performances with respect to the static case.

B. EFFICIENT NUMERICAL SOLUTION

As already mentioned, the solution of the nonlinear system (68) has to be performed at each time instant t^h, meaning that, at each time instant, an iterative scheme has to be used to find the solution $\boldsymbol{x}^{h+1}$. A *relaxed* (or *damped*) Newton-Raphson scheme [20] is used:

$$\boldsymbol{J}_{\boldsymbol{F}}(\boldsymbol{x}_k)\boldsymbol{h}_{k+1} = -\boldsymbol{F}(\boldsymbol{x}_k) \tag{69}$$

$$\boldsymbol{x}_{k+1} = \boldsymbol{x}_k + \alpha_k \boldsymbol{h}_{k+1} \tag{70}$$

where k stands for the iterations of the nonlinear solver, which has to run until convergence, and α_k is a relaxation parameter suitably chosen at every iteration to avoid overshoot of the solution.

For this specific problem, at each time instant t^h the jacobian $\boldsymbol{J}_{\boldsymbol{F}}(\boldsymbol{x}_k)$ can be written as a sum of two terms:

$$\boldsymbol{J}_{\boldsymbol{F}}(\boldsymbol{x}_k) = \boldsymbol{J}'_{\boldsymbol{F}}(\boldsymbol{x}_0) + \boldsymbol{J}''_{\boldsymbol{F}}(\boldsymbol{x}_k) \tag{71}$$

where

$$\boldsymbol{J}'_{\boldsymbol{F}}(\boldsymbol{x}_0) = \underbrace{\left[\begin{array}{cc|ccc} \boldsymbol{K} & \boldsymbol{K}_{bc} & 0 & 0 & 0 \\ \hat{\boldsymbol{S}} & \hat{\boldsymbol{S}}_{bc} & 0 & 0 & 0 \\ \hline 0 & 0 & -1 & 0 & 0 \\ 0 & 0 & 0 & -1 & 0 \\ 0 & 0 & 0 & 0 & 0 \end{array}\right]}_{\text{fixed over } k} \tag{72}$$

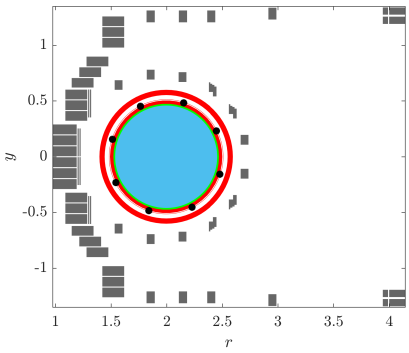

FIGURE 5. View of RFX-mod geometry (grey = active coils, red = passive conductors, blue = plasma domain) and pick-up probes (black dots).

$$\boldsymbol{J}''_{\boldsymbol{F}}(\boldsymbol{x}_k) = \underbrace{\left[\begin{array}{cc|ccc} -\mu_0 \frac{d\boldsymbol{i}}{d\boldsymbol{\psi}} & 0 & -\mu_0 \frac{d\boldsymbol{i}}{d\psi_a} & -\mu_0 \frac{d\boldsymbol{i}}{d\psi_b} & -\mu_0 \frac{d\boldsymbol{i}}{d\lambda} \\ 0 & 0 & 0 & 0 & 0 \\ \hline \boldsymbol{\chi}_a(\boldsymbol{x}) & 0 & 0 & 0 & 0 \\ \boldsymbol{\chi}_b(\boldsymbol{x}) & 0 & 0 & 0 & 0 \\ \frac{dI_t}{d\boldsymbol{\psi}} & 0 & \frac{dI_t}{d\psi_a} & \frac{dI_t}{d\psi_b} & \frac{dI_t}{d\lambda} \end{array}\right]}_{\text{to be updated at every iteration } k} \tag{73}$$

This peculiar feature of the jacobian was also typical of the formulation at the basis of FRIDA code, described in detail in [8]. Thus, also for this problem, the fixed term $\boldsymbol{J}'_{\boldsymbol{F}}(\boldsymbol{x}_0)$ depends only on the geometry of the triangulation, and it is always the same if the same mesh is considered. Consequently, it can be computed only once during a preprocessing phase and stored, allowing a more efficient implementation. On the other hand, $\boldsymbol{J}''_{\boldsymbol{F}}(\boldsymbol{x}_k)$, that has to be updated at every iteration k, is computed using a hybrid semi-analytical approach which exploits the sparsity of the original matrix $\boldsymbol{A}$. This approach is strongly parallelizable, ensuring a fast and efficient implementation, both in terms of CPU time and memory usage.

This algorithm has been implemented in the FRIDA-TD (FRIDA-*Time Domain*) code. Like the static FRIDA [8], FRIDA-TD has also been developed in the MATLAB environment, with parallel C++ subroutines for the most demanding computations.

Thanks to the efficient computation of the jacobian mentioned above, the only critical step in the entire algorithm is the correction term $\boldsymbol{h}_{k+1}$, because it requires the solution of the linear system (69). An efficient solution of this linear system is obtained by performing a LU factorization of the jacobian $\boldsymbol{J}_{\boldsymbol{F}}(\boldsymbol{x}_k)$ via the KLU algorithm [21].

In order to further speed up the computation, a Quasi-Newton method is adopted: both $\boldsymbol{J}_{\boldsymbol{F}}(\boldsymbol{x}_k)$ and $\boldsymbol{h}_{k+1}$ are not updated automatically at each iteration of the nonlinear solver, but only if the norm of the residue does not decrease sufficiently during a given iteration. By doing this, it is possible to substantially reduce the number of jacobian computations and the solution of (69).

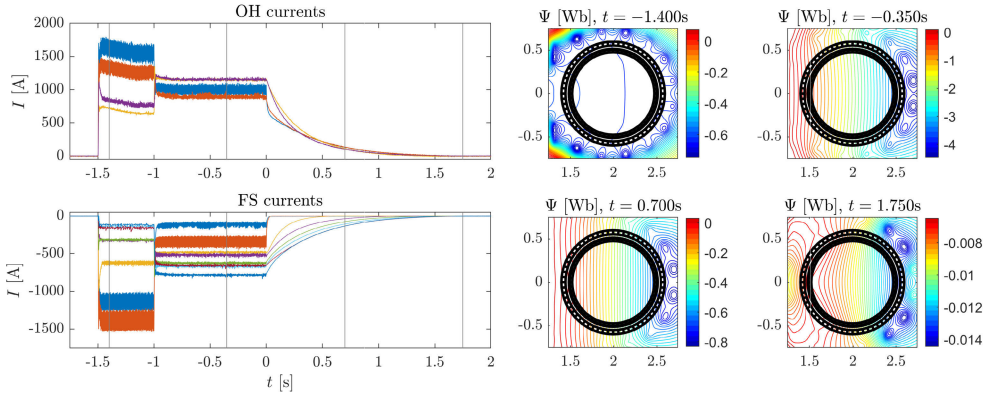

FIGURE 6. Waveforms of the current on the Ohmic Heating (OH) and Field Shaping (FS) windings, where each color refer to a different circuit, and contour plots of the poloidal flux Ψ for different time instants (these time instants are also plotted on top of OH and FS currents).

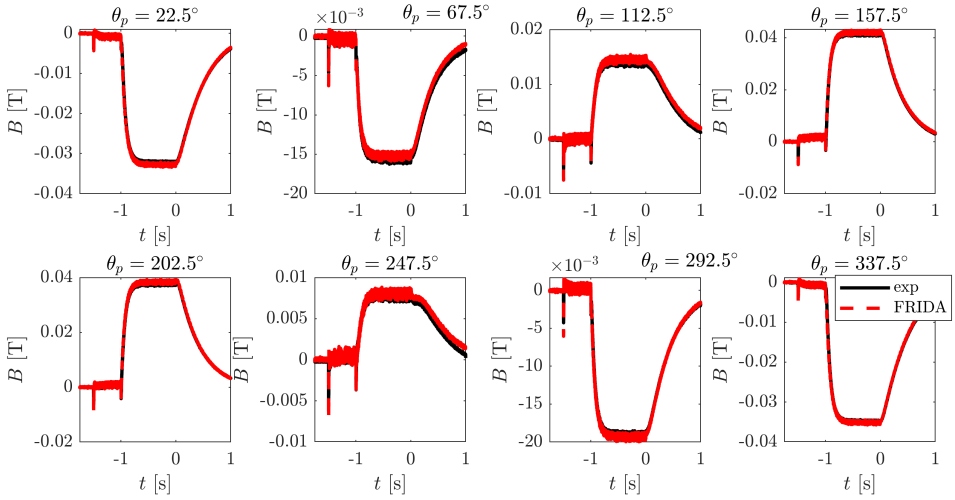

FIGURE 7. Pick-up signal: experimental (black) versus FRIDA-TD (red).

IV. VALIDATION

This section is aimed at a comprehensive and detailed validation of the FRIDA-TD code, both against synthetic data from a reference code and from experimental results.

As a preliminary test, the accuracy of the electromagnetic model without plasma (i.e. vacuum model) presented in Sec. II-B is assessed, specifically the ability to model toroidally discontinuous passive conductors (Par. II-B1). For this purpose, as a comparison, experimental data from a RFX-mod vacuum shot were considered.

In order to characterize the accuracy of the FRIDA-TD code, we firstly considered, as a reference, synthetic data from the CarMa0NL code. In addition to this, experimental data of the last part of the flat-top and the ramp-down of a RFX-mod tokamak discharge have been also considered.

All following simulations and numerical experiments have been performed on a standard Desktop machine with Intel Core i7 processor (6 cores, 2666MHz) and 16GB of memory.

A. VALIDATION OF THE VACUUM MODEL

Experimental data from a RFX-mod vacuum shot has been considered. RFX-mod had three conducting structures, the Vacuum Vessel (VV), the Plasma Stabilizing Shell (PSS), and the Toroidal Support Structure (TSS). Among these structures, both the PSS and the TSS are toroidally discontinuous and have to be modeled appropriately. A detailed description of RFX-mod load assembly can be found in [22].

The geometry of RFX-mod device can be seen in Fig. 5 (grey = active coils, red = passive conductors, blue = plasma domain). The accuracy of FRIDA-TD against experimental reference results is performed considering the signal of the ex-vessel pick-up probes installed on RFX-mod. RFX-mod had 4 arrays of pick-up coils at 4 toroidal angles, each one with 8 probes spanning a 2π angle in the poloidal direction (black dots in Fig. 5). The axisymmetric component of the pick-up measure has been obtained by averaging the signals of the 4 arrays of pick-up coils placed at different toroidal angles.

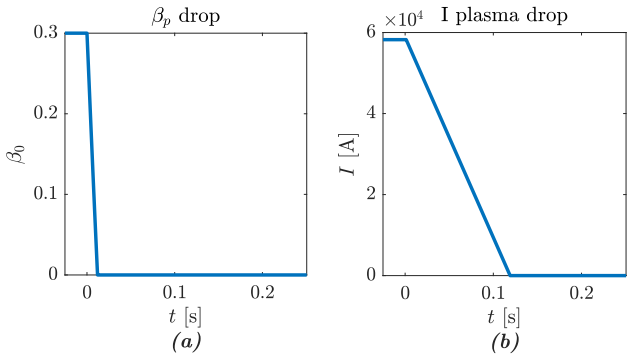

FIGURE 8. Inputs for the test cases of the validation against the CarMa0NL code. 8a): a sudden drop of the plasma poloidal beta β_p, modelled through a drop of the β_0 parameter of the parametrization (3); 8b) sudden drop of total plasma current.

The considered vacuum shot (i.e. shot no. 19051) had been performed to assess the penetration time of a vertical field through the passive conductors of RFX-mod. Figures (6) show the waveforms of the current on the Ohmic Heating (OH) and Field Shaping (FS) windings, and contour plots of the poloidal flux Ψ for different time instants (these time instants are also plotted on top of OH and FS currents in (6)).

The results are shown in Fig. 7, where the signal from the 8 pick-up probes are compared. It can be seen that the results agree well with the experimental results, highlighting that the electromagnetic model is suitable to model both toroidally continuous (VV) and discontinuous (PSS and TSS) passive conductors.

B. VALIDATION AGAINST CarMa0NL CODE

The CarMa0NL code [7] has the capability of treating self-consistently the nonlinear evolution of an axisymmetric plasma, in the evolutionary equilibrium limit, in the presence of three-dimensional (3D) volumetric conductors. CarMa0NL has been extensively validated in the latest years and can be considered one of the reference codes for addressing this kind of problem.

Two test cases are considered in this paragraph: a sudden drop of the plasma poloidal beta β_p [10], modelled through a drop of the β_0 parameter of the parametrization (3) (Fig. 8a)), in presence of toroidally *continuous* passive conductors, and a sudden drop of total plasma current (Fig. 8b), in presence of toroidally *discontinuous* passive conductors. These cases are named case 1 and 2, respectively.

Concerning the active coils, the same geometry of RFX-mod coils has been used. As passive conductor, the Plasma Stabilizing Shell (PSS, a 3mm thick copper shell) of RFX-mod is considered, while the other passive conductors (i.e. the VV and TSS) are neglected. For case 1, the PSS gap has been neglected, resulting in a toroidally *continuous* conductor. Conversely, for case 2, the PSS gap has been considered. A cut view of the three-dimensional geometry of external sources for CarMa0NL can be seen 9a.

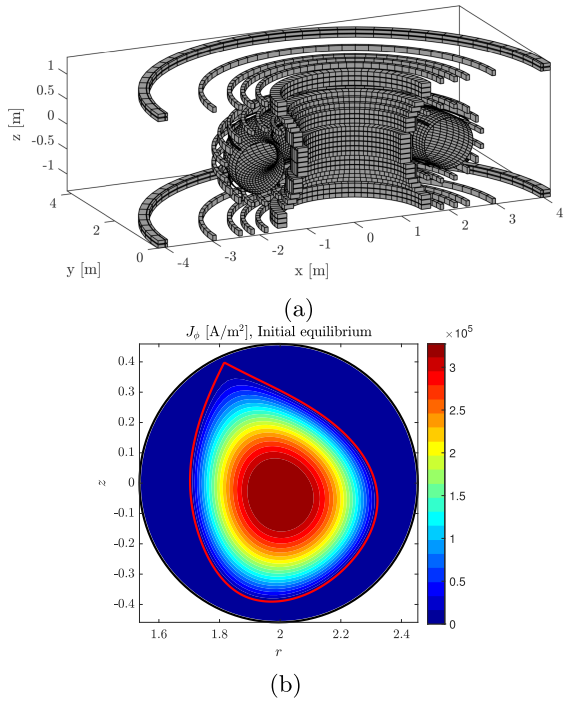

FIGURE 9. 9a geometry of external sources for CarMa0NL; 9b current density and separatrix (red) for the starting equilibrium at $t = 0$s.

For both the cases, the starting equilibrium is an RFX-mod Upper Single Null tokamak equilibrium (i.e. shot no. 36922). Figure 9b shows the current density and the separatrix (red) for this equilibrium. Since RFX tokamak equilibria with shaped cross-sections are vertically unstable [23], the aim of these tests is to trigger a Vertical Displacement Event (VDE), in order to solve and compare the evolutionary equilibrium obtained by FRIDA-TD and CarMa0NL.

case 1: the only input which varies over time is the β_0 parameter, which enters the parametrization (3) of the plasma current density. The passive conductors are toroidally continuous. The external sources (i.e. active and passive conductors) are all axisymmetric, although CarMa0NL uses a three-dimensional volumetric mesh for their description. The first comparison concerns the solution of (68), which gives the poloidal flux map at each time instant t. Figure 10 shows the solution given by FRIDA-TD (contour plot) together with the separatrix computed by CarMa0NL (red line) for 8 selected time instants. As can be seen, the FRIDA-TD solution is in excellent agreement with the CarMa0NL separatrix. The signal from the 8 pick-up probes are compared (Fig. 11). As can be seen, the results given by FRIDA-TD agree well with the CarMa0NL reference data for the entire length of the transient. In addition to this, The eddy current induced in the passive conductors, evaluated

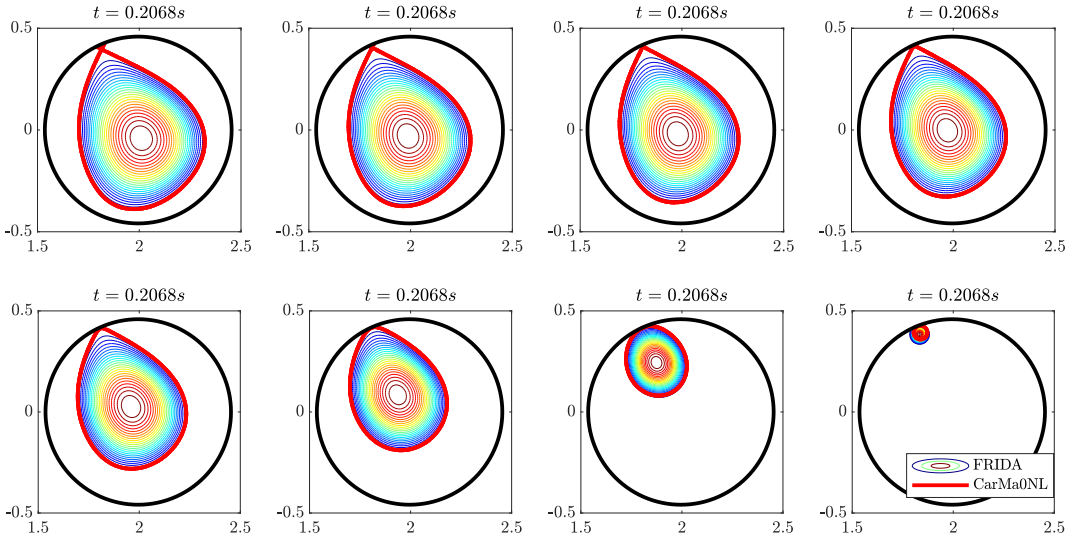

FIGURE 10. Map of the poloidal flux for various time instants during the transient: FRIDA-TD (contour plot) versus CarMa0NL (red separatrix).

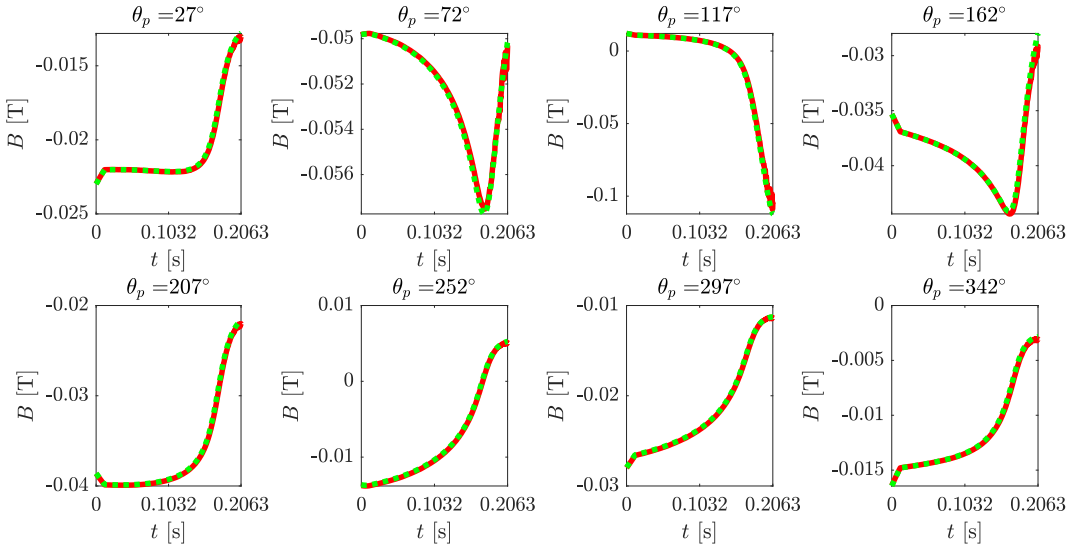

FIGURE 11. Pick-up signal: Carma0NL (green dashed) versus FRIDA-TD (red).

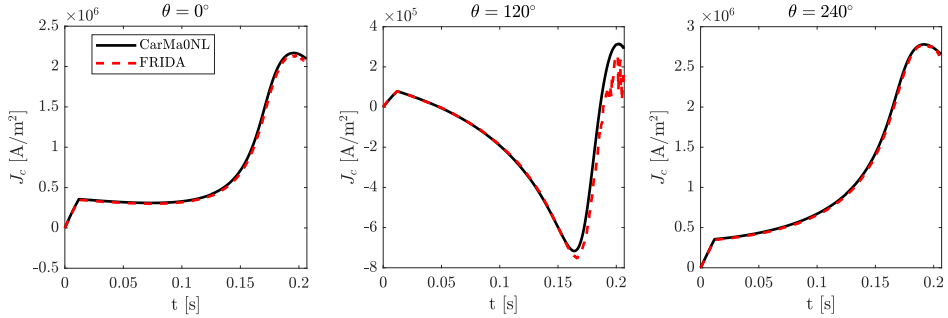

FIGURE 12. Current density in the passive conductors at three different poloidal angles: Carma0NL (black) versus FRIDA-TD (red dashed).

at three different poloidal angles, are also compared and can be seen in Fig. 12.

case 2: the total plasma current (i.e. I_p in RHS of Eq. (68)) is varied accordingly with the waveform shown in

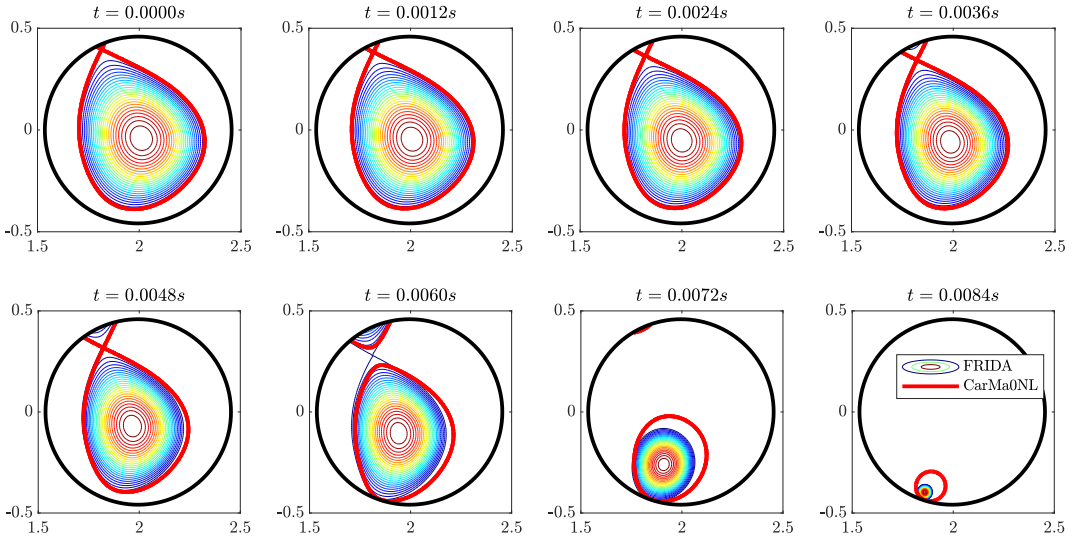

FIGURE 13. Map of the poloidal flux for various time instants during the transient: FRIDA-TD (contour plot) versus CarMaoNL (red separatrix).

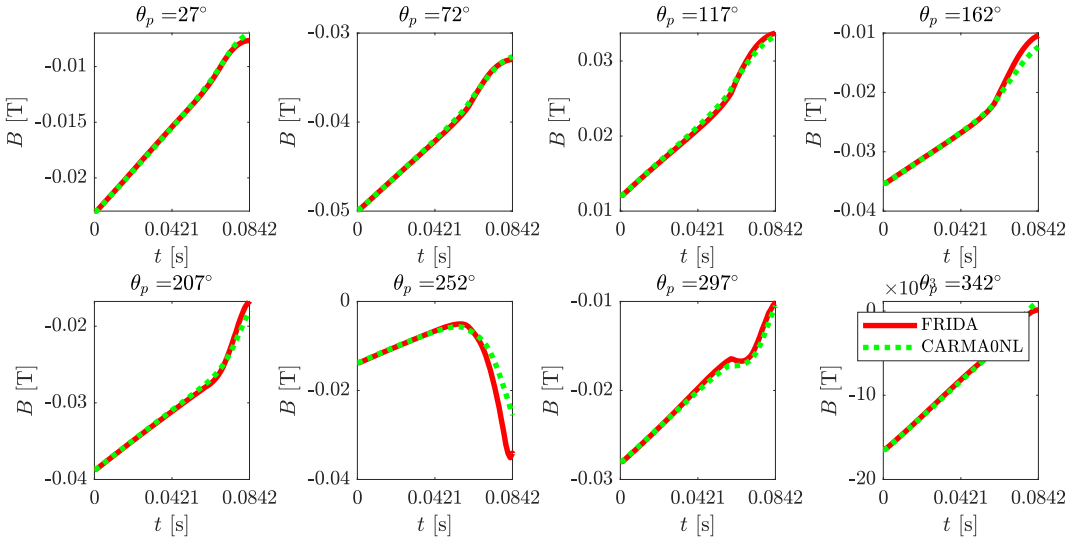

FIGURE 14. Pick-up signal: Carma0NL (green dashed) versus FRIDA-TD (red).

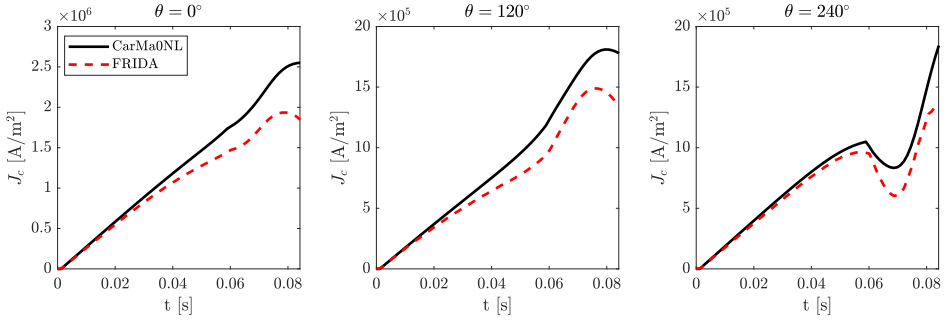

FIGURE 15. Current density in the passive conductors at three different poloidal angles: Carma0NL (black) versus FRIDA-TD (red dashed).

Fig. 8. In addition to this, a toroidally discontinuous passive shell is considered.

The poloidal flux map given by FRIDA-TD (contour plot) and CarMa0NL (separatrix, red line) are

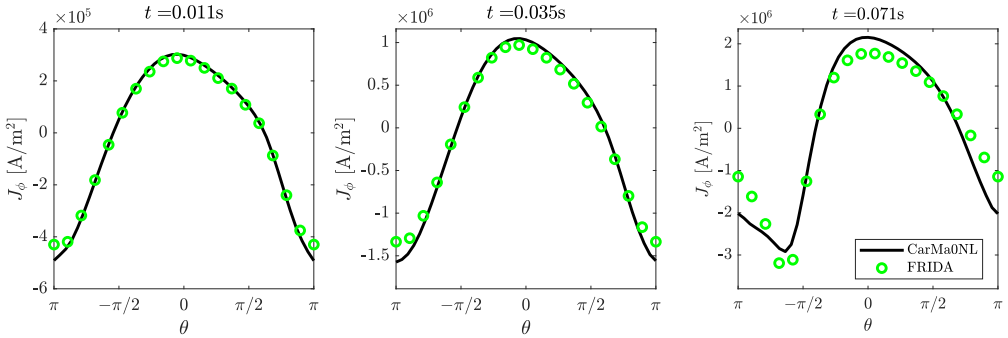

FIGURE 16. Comparison of the distribution the eddy current along the poloidal angle θ for three selected time instants.

compared in Fig. 13, showing that, although the consistency between the results is not as good as the axisymmetric case, a good agreement can be still achieved. This is highlighted also by the pick-up probes (Fig. 14). The results given by FRIDA-TD are in good agreement with CarMa0NL reference data for almost the entire length of the transient, and a small deviation occurs in the last part. This can be due to a slight underestimation of the stabilizing effect of the passive conductors if the gap is modeled with axisymmetric conductors, suggested by the fact that the downward movement of the plasma predicted by FRIDA-TD is slightly faster. This consideration is corroborated by the comparison of the eddy current induced in the passive conductors, evaluated *far from the gap* (i.e. at the opposite toroidal angle) at three different poloidal angles (Fig. 15). The eddy currents computed by FRIDA-TD are in good agreement in the first half of the VDE, while being slightly smaller in the last part of the transient. For three selected time instants, the distribution of the eddy currents along the poloidal angle θ obtained from the two codes is also compared, showing a good agreement between the results.

C. VALIDATION AGAINST RFX-MOD EXPERIMENTAL DATA

The equilibrium used in the comparison with the CarMa0NL code is an experimental equilibrium achieved in RFX-mod operating as a low current tokamak. The purpose of this paragraph is to reproduce this experimental shot with the FRIDA-TD code and compare the outcomes with the experimental data available.

The considered discharge (i.e. shot no. 36922) is an Upper Single Null (USN) discharge [24] lasting approximately 1.1s, whose equilibrium at $t = 0.6$s has been already shown in Fig. 9b. The waveforms of the currents in Ohmic Heating (OH) and Field Shaping (FS) windings, and the total plasma current, are reported in Figs. 17.

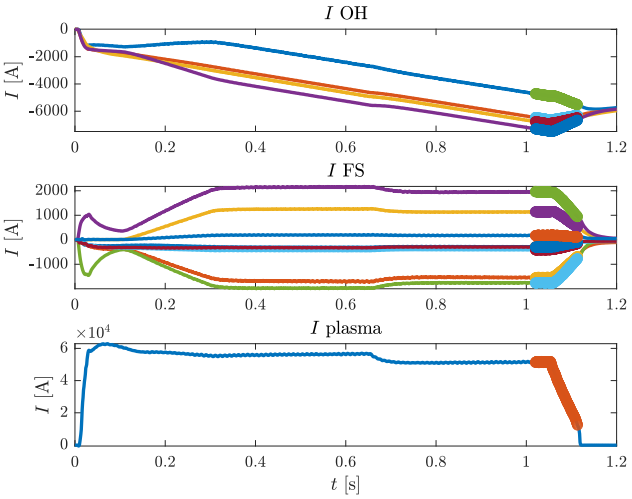

FIGURE 17. From top to bottom: waveforms of the currents in Ohmic Heating (OH) and Field Shaping (FS) windings, total plasma current. The time interval $t \in [1.02, 1.11]$s considered in the simulation is highlighted (thick).

This equilibrium, like other RFX-mod equilibria with shaped cross-sections, is characterized by having an unstable $n = 0$ mode (i.e. vertical instability), being n the toroidal mode number. The typical growth rates of such vertical instability are between 2s^{-1} and 9s^{-1} [23]. Since, unlike the RFX-mod experiment, no feedback control of the vertical position is implemented in FRIDA-TD, a Vertical Displacement Event (VDE) is expected if the timescale of the simulation is comparable with the timescale of the $n = 0$ instability. Therefore, a proper analysis of the entire shot from start-up to ramp-down would necessarily require the implementation of a feedback controller on the plasma position. For this reason, only the last part of the ramp-down phase is analyzed, in the interval $t \in [1.02, 1.11]$s (thick part in Fig. 17).

Figure 18 shows the good agreement between current density predicted by FRIDA-TD (red) and the experimental values (black) estimated following the procedure presented in [25]. The same consistency in the results can be observed also from the perturbed signal of the 8 pick-up probes (i.e. the measure at t_0 is subtracted to the signal), reported in Fig. 18b.

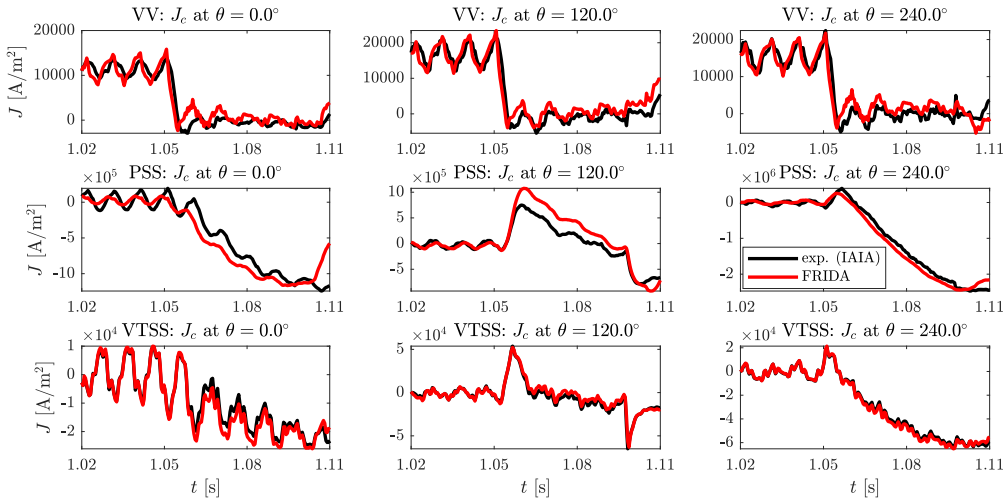

(a) Current density in the passive conductors at three different poloidal angles: experimental (black) versus FRIDA-TD (red dashed).

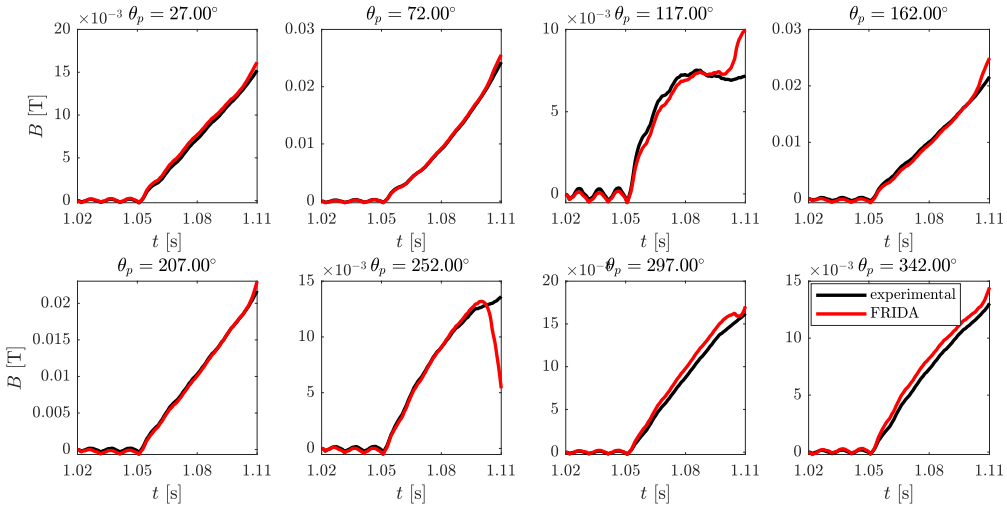

(b) Perturbation of pick-up signal: experimental (black) versus FRIDA-TD (red).

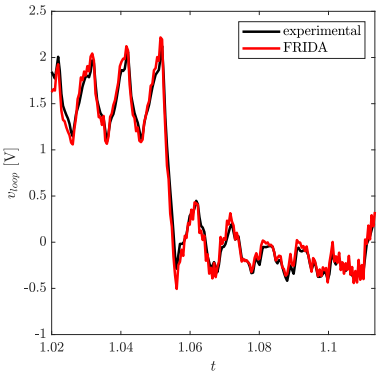

(c) loop voltage signal: experimental (black) versus FRIDA-TD (red).

FIGURE 18. **Validation of FRIDA-TD against RFX-mod experimental data.**

In addition to this, the experimental value of the loop voltage measured by the flux loops is compared to the one computed by FRIDA-TD (i.e. v_{gap} in Eqs. (26) and (28)), and is shown in Fig. 18c.

V. CONCLUSION AND FURTHER DEVELOPMENTS

In this paper, an efficient numerical tool for solving the problem of transient nonlinear evolution of plasma equilibrium in presence of eddy currents is presented. The code is named FRIDA-TD (FRIDA-*Time Domain*) after the existing FRIDA (FRee-boundary Integro-Differential Axisymmetric) static equilibrium solver. Two different approaches are exploited to efficiently deal with the problem: Finite Element Method - Boundary Element Method (FEM-BEM) for plasma equilibrium, and Axisymmetric Volume Integral (AVI) formulation for eddy currents.

After describing in detail the mathematical formulation used to couple the free-boundary equilibrium and eddy current problems, FRIDA-TD has been at first successfully compared with the well-established CarMaoNL code. Furthermore, FRIDA-TD has been validated against experimental data by accurately replicating the ramp-down phase of a RFX-mod tokamak discharge.

The presented FRIDA-TD is a fast and flexible tool suitable for engineering-oriented purposes, such as the design of Tokamak devices, set up of plasma operations, prediction of performance scenarios, and the design of feedback control systems. Further work will be devoted to the implementation of plasma position and shape feedback controllers, to allow the simulation of an entire shot from start-up to rump-down phases.

APPENDIX
USEFUL RELATIONS

Additional relations mentioned in Sec. II-B for the axisymmetric volume integral formulation of eddy current problem are reported in this appendix.

$$V_{ij} = \int_{\Omega_c} w_i(\vec{r}) w_j(\vec{r}) d\Omega \tag{74}$$

$$U_{ij} = \int_{\Omega_c} 2\pi r w_i(\vec{r}) w_j(\vec{r}) d\Omega \tag{75}$$

$$\tilde{G}_{bc,ij} = \frac{1}{2\pi} \int_{\Omega_{cj}} 2\pi r w_i(\vec{r}) \left[\frac{\mu_0}{4\pi} \int_{V_c} \frac{w_j(\vec{r}')}{|\vec{r} - \vec{r}'|} dV' \right] d\Omega \tag{76}$$

where Ω_{ci} is the local support of the *ith* node belonging to the passive conductors, i.e. all the triangles which shares such node, and χ_{s_i} is a constant current density chosen in order to obtain a unitary total current on the coil.

EQUATION FOR PLASMA RESPONSE

As pointed out in Par. III-A, the coupling between FB-PEP and eddy current problem is based on the introduction of a coupling surface S_e, whose trace on the poloidal plane is labeled Γ_{eq}. The coupling surface has to be chosen without intersecting neither the plasma nor the passive structures, and all these structures must be outside it. A sketched view of this configuration can be seen in Fig. 4. An equivalent current $\boldsymbol{i}_{eq}$ flows on the coupling surface, producing outside it the same magnetic flux of the actual plasma equilibrium [26].

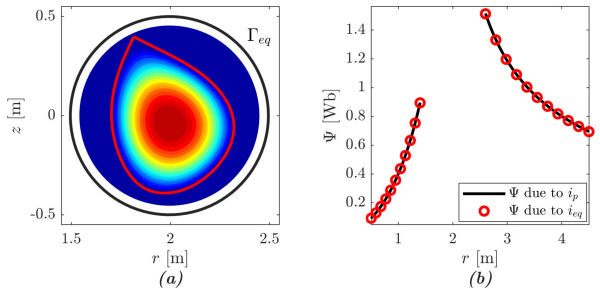

FIGURE 19. 19a): plasma current density and coupling surface Γ_{eq} (black); 19b): comparison between total flux produced by the actual plasma current i_p and by the equivalent current i_{eq} on Γ_{eq}.

The equivalent surface current, rather than nodal plasma currents $\boldsymbol{i}_p$, is then used to evaluate the mutual coupling between plasma and passive conductors, which is computed via relation (16). Since $N_{eq} \ll N_n$, the size of (16) reduces dramatically with respect to the case of considering directly the nodal plasma currents $\boldsymbol{i}_p$.

Given the nodal current densities $\boldsymbol{g}_p$ (i.e. defined on the mesh nodes) for a certain equilibrium, the equivalent current *density* $\boldsymbol{j}_{eq}$ on Γ_{eq} can be computed rigorously as [26]:

$$\boldsymbol{j}_{eq} = -\frac{1}{\mu_0 r} \nabla \psi^* \cdot \vec{\boldsymbol{n}} \tag{77}$$

here $\psi^* = \psi - \psi_{vac}$, being ψ is the solution of (1) with the actual plasma current density as source and the related boundary conditions, and ψ_{vac} is the solution with zero source term (*vacuum* solution) but imposing the same boundary conditions as for the previous case.

The approach exploited in this work is slightly different, but still based on the constrain that the equivalent currents produce, outside the coupling surface, the same magnetic field produced by the plasma. For this reason, a set of N_{eq} points, located *just outside* the coupling surface, are chosen, defining a target surface Γ_{target}. The Green matrix[2] $\boldsymbol{G}_{tp} = \boldsymbol{G}(\vec{\boldsymbol{r}}_{target}, \vec{\boldsymbol{r}}_p)$ and $\boldsymbol{G}_{teq} = \boldsymbol{G}(\vec{\boldsymbol{r}}_{target}, \vec{\boldsymbol{r}}_{eq})$ between the equivalent currents and the target points are then computed. By imposing that:

$$\boldsymbol{G}_{tp} \boldsymbol{i}_p = \boldsymbol{\psi}_{target} = \boldsymbol{G}_{teq} \boldsymbol{i}_{eq} \tag{79}$$

it is possible to obtain the equivalent surface current:

$$\boldsymbol{i}_{eq} = \boldsymbol{G}_{teq}^{-1} \boldsymbol{G}_{tp} \boldsymbol{i}_p = \boldsymbol{T}_{eq} \boldsymbol{i}_p \tag{80}$$

where $\boldsymbol{T}_{eq}$ is a $N_{eq} \times N_n$ already introduced in (30)-(31)-(32). The matrix $\boldsymbol{G}_{teq}$ is square because N_{eq} target point are chosen, thus its inverse can be computed exactly. We stress

[2]The Green matrix gives the flux produced by a filamentary unit current flowing through a circular loop at $\boldsymbol{r}$ onto a given point $\boldsymbol{r}'$, and is defined as [13]:

$$G(\boldsymbol{r}', \boldsymbol{r}) = \frac{\mu_0 \sqrt{r r'}}{2\pi k(\vec{\boldsymbol{r}}, \vec{\boldsymbol{r}}')} \left[\left(2 - k^2(\vec{\boldsymbol{r}}, \vec{\boldsymbol{r}}')\right) K\left(k(\vec{\boldsymbol{r}}, \vec{\boldsymbol{r}}')\right) - 2E\left(k(\vec{\boldsymbol{r}}, \vec{\boldsymbol{r}}')\right) \right], \tag{78}$$

where $k^2(\vec{\boldsymbol{r}}, \vec{\boldsymbol{r}}') = \frac{4 r r'}{(r+r')^2 + (z-z')^2}$, and $K(k)$, $E(k)$ are the complete elliptic integrals of the first and second kind, respectively.

the point that, by using this approach, it is not necessary to compute ψ^*, which requires two solutions of Eq. (1). The computation of $\boldsymbol{T}_{eq}$ can be performed beforehand during a preprocessing phase, and need to be done only once, as such matrix is always the same if the mesh does not change.

Figure 19a shows the plasma current density and coupling surface Γ_{eq} (black), and, in Fig. 19b, a comparison between the total flux produced by the actual plasma current $\boldsymbol{i}_p$ (black) and by the equivalent current $\boldsymbol{i}_{eq}$ on Γ_{eq} (red circles).

ACKNOWLEDGMENT

The authors would like to thank Dr. D. Terranova for the numerous hints and suggestions that substantially improved the quality of the work.

REFERENCES

[1] R. Albanese, J. Blum, and O. D. Barbieri, "Numerical studies of the next European torus via the PROTEUS code," in *Proc. 12th Conf. Numer. Simulation Plasmas*, 1987.
[2] R. R. Khayrutdinov and V. E. Lukash, "Studies of plasma equilibrium and transport in a tokamak fusion device with the inverse-variable technique," *J. Comput. Phys.*, vol. 109, no. 2, pp. 193–201, 1993.
[3] S. C. Jardin, N. Pomphrey, and J. Delucia, "Dynamic modeling of transport and positional control of tokamaks," *J. Comput. Phys.*, vol. 66, no. 2, pp. 481–507, Oct. 1986.
[4] P. Barabaschi, "The MAXFEA code," in *Proc. ITER EDA Plasma Control Tech. Meeting*, 1993.
[5] H. Heumann, J. Blum, C. Boulbe, B. Faugeras, G. Selig, J.-M. Ané, S. Brémond, V. Grandgirard, P. Hertout, and E. Nardon, "Quasi-static free-boundary equilibrium of toroidal plasma with CEDRES++: Computational methods and applications," *J. Plasma Phys.*, vol. 81, no. 3, Jun. 2015, Art. no. 905810301.
[6] R. Albanese, R. Ambrosino, and M. Mattei, "CREATE-NL+: A robust control-oriented free boundary dynamic plasma equilibrium solver," *Fusion Eng. Des.*, vols. 96–97, pp. 664–667, Oct. 2015.
[7] F. Villone, L. Barbato, S. Mastrostefano, and S. Ventre, "Coupling of nonlinear axisymmetric plasma evolution with three-dimensional volumetric conductors," *Plasma Phys. Controlled Fusion*, vol. 55, Jul. 2013, Art. no. 095008.
[8] N. M. Bonotto, N. D. Abate, N. P. Bettini, and F. Villone, "A coupled FEM-BEM approach for the solution of the free-boundary axi-symmetric plasma equilibrium problem," *Commun. Comput. Phys.*, vol. 31, no. 1, pp. 27–59, Jun. 2022.
[9] P. Piovesan, "RFX-mod: A multi-configuration fusion facility for three-dimensional physics studies," *Phys. Plasmas*, vol. 20, no. 5, May 2013, Art. no. 056112.
[10] J. P. Freidberg, *Ideal MHD*. Cambridge, U.K.: Cambridge Univ. Press, 2014.
[11] J. L. Luxon and B. B. Brown, "Magnetic analysis of non-circular cross-section tokamaks," *Nucl. Fusion*, vol. 22, no. 6, pp. 813–821, Jun. 1982.
[12] J. Blum, *Numerical Simulation and Optimal Control in Plasma Physics*. Hoboken, NJ, USA: Wiley, 1989.
[13] K. Lackner, "Computation of ideal MHD equilibria," *Comput. Phys. Commun.*, vol. 12, no. 1, pp. 33–44, Sep. 1976.
[14] D. Knoll and D. Keyes, "Jacobian-free Newton–Krylov methods: A survey of approaches and applications," *J. Comput. Phys.*, vol. 193, no. 2, pp. 357–397, 2004.
[15] C. Geuzaine and J.-F. Remacle, "Gmsh: A 3-D finite element mesh generator with built-in pre- and post-processing facilities," *Int. J. Numer. Methods Eng.*, vol. 79, no. 11, pp. 1309–1331, Sep. 2009.
[16] F. Gnesotto, P. Sonato, W. R. Baker, A. Doria, F. Elio, M. Fauri, P. Fiorentin, G. Marchiori, and G. Zollino, "The plasma system of RFX," *Fusion Eng. Des.*, vol. 25, no. 4, pp. 335–372, Jan. 1995.
[17] P. Bettini, M. Cavinato, and F. Trevisan, "Dynamic identification of plasma magnetic contour in fusion machines," *Nucl. Fusion*, vol. 45, no. 1, pp. 1–12, Jan. 2005.
[18] F. Villone, A. G. Chiariello, S. Mastrostefano, A. Pironti, and S. Ventre, "GPU-accelerated analysis of vertical instabilities in ITER including three-dimensional volumetric conducting structures," *Plasma Phys. Controlled Fusion*, vol. 54, no. 8, Aug. 2012, Art. no. 085003.
[19] M. Bonotto, Y. Q. Liu, F. Villone, L. Pigatto, and P. Bettini, "Expanded capabilities of the CarMa code in modeling resistive wall mode dynamics with 3-D conductors," *Plasma Phys. Controlled Fusion*, vol. 62, no. 4, Apr. 2020, Art. no. 045016.
[20] M. A. Crisfield, "Accelerating and damping the modified Newton-raphson method," *Comput. Struct.*, vol. 18, no. 3, pp. 395–407, Jan. 1984. [Online]. Available: http://www.sciencedirect.com/science/article/pii/0045794984900592
[21] T. A. Davis and E. P. Natarajan, "Algorithm 907: KLU, a direct sparse solver for circuit simulation problems," *ACM Trans. Math. Softw.*, vol. 37, no. 3, pp. 1–17, Sep. 2010.
[22] P. Sonato, G. Chitarin, P. Zaccaria, F. Gnesotto, S. Ortolani, A. Buffa, M. Bagatin, W. R. Baker, S. D. Bello, P. Fiorentin, L. Grando, G. Marchiori, D. Marcuzzi, A. Masiello, S. Peruzzo, N. Pomaro, and G. Serianni, "Machine modification for active MHD control in RFX," *Fusion Eng. Des.*, vols. 66–68, pp. 161–168, Sep. 2003.
[23] D. Abate, G. Marchiori, and F. Villone, "Plasma shape effect on the n = 0 stability of RFX-modshaped tokamak plasmas," *Nucl. Fusion*, vol. 59, no. 6, may 2019, Art. no. 066027, doi: 10.1088/1741-4326/ab0fd1.
[24] G. Marchiori, C. Finotti, O. Kudlacek, F. Villone, P. Zanca, D. Abate, R. Cavazzana, G. L. Jackson, T. C. Luce, and L. Marrelli, "Design and operation of the RFX-mod plasma shape control system," *Fusion Eng. Des.*, vol. 108, pp. 81–91, Oct. 2016.
[25] A. Cenedese, P. Bettini, and M. Bonotto, "Model-based approach for magnetic reconstruction in axisymmetric nuclear fusion machines," *IEEE Trans. Plasma Sci.*, vol. 46, no. 3, pp. 636–644, Mar. 2018.
[26] V. D. Pustovitov, "Decoupling in the problem of tokamak plasma response to asymmetric magnetic perturbations," *Plasma Phys. Controlled Fusion*, vol. 50, no. 10, Oct. 2008, Art. no. 105001.

MATTEO BONOTTO was born in Marostica, Italy, in 1990. He received the graduate degree in electrical engineering from the University of Padua, Italy, in 2015, and the Ph.D. degree in fusion science and engineering from the University of Padua and the Instituto Superior Técnico of Lisbon, Portugal, in 2019. He is currently a Postdoctoral Research Scientist with Consorzio RFX, Padua, and Istituto Nazionale di Fisica Nucleare–Laboratori Nazionali di Legnaro (INFN-LNL), Legnaro, Italy. His research interests include magnetic confinement fusion and spanning multiple fields, such as electromagnetism, computational physics, control theory, plasma physics, and artificial intelligence.

DOMENICO ABATE received the degree in energy engineering, the M.Sc. degree in electrical engineering, and the Ph.D. degree in fusion science and engineering from the University of Padua, in 2012, 2014, and 2018, respectively. He has been a Research Scientist with Consorzio RFX, Padua, since 2020, and during this time, he also worked as a guest researcher in many European laboratories. His research interests include MHD plasma equilibrium, mathematical optimization, magnetic diagnostics, and control of magnetized plasmas for fusion experiments.

PAOLO BETTINI (Senior Member, IEEE) received the M.S. and Ph.D. degrees in electrical engineering from the University of Padua, Italy, in 1994 and 1998, respectively. He was an Associate Professor of electrical engineering with the University of Udine, from 2005 to 2009, and the University of Padua, from 2009 to 2021. He was the Director of the International Ph.D. Program in fusion science and engineering, from 2014 to 2020. He is currently a Professor of electrical engineering with the University of Padua, where he is also the Director of the Research Center on Nuclear Fusion. He has coauthored more than 150 indexed scientific publications on several topics concerning the computation of electromagnetic fields and magnetic confinement fusion.

ANTONIO IAIUNESE was born in Caserta, Italy, in 1994. He received the M.S. degree in electronic engineering from the University of Campania "Luigi Vanvitelli," in 2020. He is currently pursuing the Ph.D. degree (joint-Ph.D.) in fusion science and engineering with the University of Padua and the University of Naples Federico II. His research interests include numerical methods, modeling of magnetic components of Tokamak devices, the study of the interaction between electromagnetic fields, and conductive structures.

NICOLA ISERNIA received the M.Sc. degree (cum laude) in electrical engineering from the University of Naples Federico II, in 2018, and the Ph.D. degree from the Information Technology and Electrical Engineering School of Federico II, in 2022, with a thesis dealing with the electromagnetic interaction of fusion plasmas with external conductors. During his Ph.D. studies, he was interested in magnetic confinement fusion experiments, collaborating with several research institutes across Europe, mainly the Institute of Plasma Physics of the Czech Academy of Sciences, the Culham Centre for Fusion Energy, and the Max-Planck Institute for Plasma Physics in Garching bei Munchen. His actual research interests include the integration of MHD models of fusion plasmas with MQS models for external 3-D conductors and applications of simplified mass-less plasma models for studying the consequences of hard-to-predict disruptions in tokamak experiments. He is currently a Research Fellow with the Department of Electrical Engineering and Information Technology, Dipartimento di Ignegneria Elettrica e Tecnologie dell'Informazione, University of Naples Federico II.

FABIO VILLONE received the graduate degree (magna cum laude) in electronic engineering from the University of Naples Federico II, in 1994, and the Ph.D. degree in industrial engineering from the University of Cassino, in 1997. He was an Associate Professor with the University of Cassino, from 2001 to 2007, where he was a Full Professor with the University of Cassino, from 2007 to 2017. Since 2017, he has been a Full Professor with University of Naples Federico II. He coauthored more than 300 articles in international journals, book chapters, and contributions to international conferences. His research interests include magnetic confinement fusion, ranging from MHD modeling to disruption studies, to plasma magnetic control and diagnostics. Since 2008, he has been the Chairperson and the coordinator of several committees and organizations, national and international, operating in the field of magnetic confinement fusion.

Open Access funding provided by 'Università degli Studi di Padova' within the CRUI CARE Agreement